Revealing the Heterogeneity of T Cells in a Relapsed Hodgkin Lymphoma Patient Treated with Immunotherapy using Single-cell RNA Sequencing

Matthew Salaciak

Division of Experimental Medicine
McGill University, Montreal, Canada
August 2022

A thesis submitted to McGill University in partial fulfillment of the requirements of the degree of Master of Science Experimental Medicine.

List of Abbreviations

AAVD	Brentuximab vedotin, doxorubicin, vinblastine, and dacarbazine
ABVD	Doxorubicin, bleomycin, vinblastine, and dacarbazine
APC	Antigen presenting cell
ASCT	Autologous stem cell transplant
BCR	B cell receptor
BEAM	Carmustine, etoposide, cytarabine, and melphalan
BOB.1	POU Class 2 Homeobox Associating Factor 1
BV	Brentuximab vedotin
CD15	Fucosyltransferase 4
CD244	Natural killer Cell Type I Receptor Protein 2B4
CD30	Tumor Necrosis Factor Receptor Superfamily, Member 8
CD4	T-Cell Surface Glycoprotein CD4
CD45	Protein Tyrosine Phosphatase Receptor Type C
CD62L	L-selectin (SELL)
CD8	T-Cell Surface Glycoprotein CD8
cDC	Conventional dendritic cell
cHL	Classical Hodgkin Lymphoma
CT	Computed tomography
CTLA-4	Cytotoxic T-Lymphocyte Associated Protein 4
CX3CL1	Fractalkine
CX3CR1	Fractalkine receptor
cyTOF	Mass cytometry by time of flight
DEGS	Differentially expressed genes
DNA	Deoxyribonucleic acid
G2/M	G2-phase checkpoint
GDP	Gemcitabine, dexamethasone, and cisplatin
GZMB	Granzyme B
GZMK	Granzyme K
HAVCR2	Hepatitis A Virus Cellular Receptor 2 / TIM3
HL	Hodgkin Lymphoma
HRS	Hodgkin and Reed-Sternberg cell
ICI	Immune checkpoint inhibitor
IL-7R	Interleukin-7 receptor
iRAE	Immune related adverse events
KNN	K-nearest Neighbors
LAG3	Lymphocyte-activation gene 3
LDCHL	Lymphocyte-depleted classic Hodgkin Lymphoma
LP	Lymphocyte predominant
LRCHL	Lymphocyte-rich classic Hodgkin Lymphoma
MCCHL	Mixed cellularity classic Hodgkin Lymphoma
MHC	Major histocompatibility complex
NF-κB	Nuclear factor kappa B
NK	Natural killer cell
NLPHL	Nodular Lymphocyte Predominant

NSCHL	Nodular Sclerosis classic Hodgkin Lymphoma
NSCLC	Non-small cell lung cancer
OCT2	Solute carrier family 22 member 2
PBMC	Peripheral blood mononuclear cell
PCA	Principal component analysis
PD-1	Program cell death protein 1
PD-L1	Program cell death ligand 1
pDC	Plasmacytoid dendritic cell
PET	Positron emission tomography
PRDM1	B lymphocyte-induced maturation protein-1 (BLIMP-1)
scRNA-seq	Single-cell RNA sequencing
TAM	Tumor-associated macrophages
TBX21	T-Box Transcription Factor 21(TBET)
TCF7	Transcription Factor 7 (TCF1)
Tcm	Central memory T cell
TCR	T cell receptor
Tem	Effector memory T cell
Tex	Terminal exhausted T cell
Tfh	Follicular helper T cell
Th1	T helper type 1
Th17	T helper type 17
Th2	T helper type 2
Th22	T helper type 22
Th9	T helper type 9
TIGIT	T Cell Immunoreceptor with Ig And ITIM Domains
TME	Tumor microenvironment
Tpex	Precursor exhausted T cell
Treg	Regulatory T cell
Trm	Tissue resident memory T cell
Tscm	Memory stem T cell
Tte	Terminal effector T cell
UMAP	Uniform manifold approximation and projection
UMI	Unique molecular identifier
WGCNA	Weighted gene co-expression network analysis

Abstract

Title: Revealing the Heterogeneity of T Cells in a Relapsed Hodgkin Lymphoma Patient Treated with Immunotherapy using Single-cell RNA Sequencing.

Introduction: Classical Hodgkin lymphoma (cHL) is the most common lymphoma affecting young adults. While cHL is curable in ~60% of patients with chemotherapy, relapse remains an important issue. The most active agents are programmed cell death protein 1 (PD-1) inhibitors in this setting. Hodgkin and Reed-Sternberg (HRS) cells orchestrate their microenvironment to favour their growth and use PD-1/PD-L1 immune checkpoint axis to avoid immune surveillance. PD-1 inhibitors can be effective, but the mechanisms of response are not understood. To our knowledge, previous studies using single-cell transcriptomics to characterize PD-1 inhibitor response have been exclusively carried out in solid tumor cancers but not in cHL. We hypothesize that this technology could identify mechanisms of resistance to PD-1 inhibitors in HL. Our aim is to identify the transcriptomic changes in immune subsets in a cHL patient during PD-1 inhibitor treatment.

Methods: We performed single-cell RNA sequencing (scRNA-seq) and simultaneous immune profiling using 10x Genomics Chromium Single Cell V(D)J enrichment, for Human T cell receptor (TCR), of peripheral blood mononuclear cells (PBMCs) from one relapsed HL patient treated with PD-1 inhibitor pembrolizumab. Samples were collected from six treatment time points of five discrete disease states: treatment naïve, remission, relapse, treatment rechallenge, and disease progression. Bulk TCR sequencing was performed on available PBMCs and tumor tissue samples. Downstream scRNA-seq analysis was completed using Seurat and Scanpy along with Immunearch, MiXCR, and Scirpy for TCR analysis.

Results: Unsupervised clustering resulted in nine immune cell subsets, where T cells showed most significant expression changes. Next, we subset T cells and integrated TCR datasets for analysis. T cell clones from tumor tissue samples were identified in both bulk and single-cell PBMCs TCR data sets. At relapse, an increase in CD8+ T cells inversed the CD4+/CD8+ ratio, an expansion of a CD8+ clonotype and expression of exhaustion related markers were observed. Gene co-expression network analysis of CD8+ T cells revealed two signatures related to stem-memory or terminal effector-like phenotypes. These signatures were either highly expressed or formed a gradient of expression. Expanded tumor tissue clones had preference for stem-memory-

like T cell clusters while PBMCs clones had preference for terminal effector-like clusters. Both signatures revealed T cells that expressed markers of precursor or terminal exhaustion.

Conclusions: Using scRNA-seq and TCR analysis to profile the peripheral immune cells of a cHL patient treated with PD-1 inhibitor can be useful to identify dynamic immune cell changes. Furthermore, tracking specific clonotypes present in the peripheral blood and resolving T cell heterogeneity into transcriptional signatures may provide insight into functional changes of T cells during response, relapse, and progression. We plan to validate the transcriptomic changes of multiple exhaustion markers to identify potential targets of therapy that can be used in HL patients in combination with PD-1 inhibitors or post PD-1 inhibitor relapse.

Résumé

Titre: Révélation de l'hétérogénéité des cellules T chez un patient atteint d'un Lymphome Hodgkinien récidivant et traité par immunothérapie, grâce au séquençage de l'ARN unicellulaire.

Introduction: Le Lymphome Hodgkinien classique (LHC) est le lymphome le plus fréquent chez les jeunes adultes. Bien que la chimiothérapie permette de guérir le LHC chez environ 60 % des patients, la rechute reste un problème important. Dans ce cas, les agents les plus actifs sont les inhibiteurs de la protéine de mort cellulaire programmée 1 (PD-1). Les cellules de Hodgkin et Reed-Sternberg (HRS) manipulent leur micro environnement pour favoriser leur croissance et utilisent des points de contrôle immunitaire PD-1/PD-L1 pour éviter la surveillance immunitaire. Les inhibiteurs de PD-1 peuvent être efficaces, mais les mécanismes de la réponse ne sont pas bien compris. Les études précédentes qui utilisent la transcriptomique unicellulaire pour caractériser la réponse aux inhibiteurs PD-1 ont été réalisées avec les cancers de tumeurs solides, mais pas dans le cas des LHC. Nous croyons que cette technologie pourrait permettre d'identifier les mécanismes de résistance aux inhibiteurs PD-1 dans le LHC. L'objectif est d'identifier les changements transcriptomiques dans les groupes immunitaires d'un patient atteint de LCH au cours du traitement par inhibiteur PD-1.

Méthodes: Nous avons séquencé un ARN unicellulaire (scRNA-seq) et un profilage immunitaire à l'aide de l'enrichissement V(D)J unicellulaire 10x Genomics Chromium pour le récepteur des cellules T humaines (TCR) et des cellules mononucléaires du sang périphérique (PBMC) chez un patient atteint de LH en rechute traité par l'inhibiteur PD-1 pembrolizumab. Les échantillons ont été prélevés à six moments au cours du traitement dans cinq états pathologiques : naïf de traitement, rémission, rechute, reprise du traitement et progression de la maladie. Le séquençage TCR en vrac a été effectué sur les PBMC et les échantillons de tissu tumoral. L'analyse de données a été réalisée à l'aide de Seurat et Scanpy, Immunearch, MiXCR et Scirpy.

Résultats: Le regroupement non-supervisé a permis de créer neuf groupes de cellules immunitaires: les cellules T présentant les changements d'expression les plus significatifs. Nous avons sous-divisé les cellules T et intégré les ensembles de données TCR pour l'analyse. Les clones de cellules T provenant d'échantillons de tissus tumoraux ont été identifiés dans les

ensembles de données TCR des PBMC en vrac et unicellulaires. Lors de la rechute, on a observé une inversion de la proportion CD4+/CD8+, une expansion d'un clonotype CD8+ et l'expression de marqueurs liés à l'épuisement. L'analyse du réseau de co-expression génétique des cellules T CD8+ a révélé deux signatures liées aux phénotypes de type mémoire-souche ou d'effecteur terminal. Ces signatures étaient fortement exprimées ou avaient formé une gamme d'expressions. Les clones de tissus tumoraux avaient une préférence pour les groupes de cellules T de type mémoire-souche tandis que les clones de PBMC avaient une préférence pour les groupes de type effecteur terminal. Les deux signatures ont révélé des cellules T qui exprimaient des marqueurs d'épuisement précurseur ou terminal.

Conclusions: L'utilisation de scRNA-seq et de l'analyse TCR pour établir le profil des cellules immunitaires périphériques d'un patient atteint de LCH traité par un inhibiteur PD-1 peut être utile pour identifier les changements dynamiques des cellules immunitaires. Le suivi des clonotypes spécifiques présents dans le sang périphérique et la résolution de l'hétérogénéité des cellules T en signatures transcriptionnelles peuvent éclairer des changements fonctionnels des cellules T au cours de la réponse, de la rechute et de l'épuisement. Nous prévoyons valider les changements transcriptomiques de plusieurs marqueurs d'épuisement afin d'identifier des cibles potentielles de thérapie qui peuvent être utilisées chez les patients atteints de LHC.

Table of Contents

List of Figures and Tables

Acknowledgements

Firstly, this work would not have been possible without the help and support of many individuals. I am forever grateful and thankful to be surrounded by such incredible people throughout all my endeavours. All my personal growth is thanks to you all.

To my parents, sister, and Emma, without your limitless love and support, I would not be the person I am today. I am beyond lucky to always have you all by my side, picking me up when I'm down and pushing me when I'm stuck. I will be forever indebted.

To my mom, your courageous battle with leukemia was the sole reason I decided to change my life to pursue cancer research. When I think about you, I am always reminded of how thoughtful, selfless, and caring of a person you were. The power of your love and passing will always inspire me and remind me why I am doing this. This thesis is dedicated to you.

To Dr. Johnson, you took a chance on me, and it forever changed my life. You gave me an opportunity to pursue my dreams and did so with all the support and mentorship one could give. I cannot imagine where I would be without you. You are a constant source of inspiration and aspiration. I will never be able to thank you enough.

To Dr. Mercier, your, kindness, mentorship, and willingness to help me was one of the most important factors throughout my journey. You introduced me to bioinformatics and took all the time needed to help me bridge my love for computer science to biology. Your support and words of encouragement to pursue my goals reassures me that I belong on this path. Thank you for seeing my potential and for always being there for me.

To Dr. Haliotis, your warmth, compassion and creativity influences me every day. Your selflessness to dedicate so much time to work with me has contributed to some of the most important and impactful experiences. You introduced me to the beauty of hemopathology while sharing your love to teach. I am beyond lucky and thankful to have such a mentor.

To Ryan, Liliana, Abod and Moneeza from the Johnson lab, and Dr. Koren Mann, Dr. Sonia Del Rincon, Madelyn, and Tho, I could have not asked for a better group of individuals to learn from and grow next to. Thank you all for always being so generous with your time and always being there to help me when needed.

To my thesis advisory committee, thank for your encouragement, thoughtful questions and help throughout my project.

To my friends, I am so happy to have you all in my life and by my side throughout it all.

Contribution of Authors

Dr. Nathalie Johnson provided supervision throughout the entirety of this thesis project.

Introduction literature review: This chapter was written entirely by Matthew Salaciak

Methods/Results: Liliana Stoica managed and processed the samples. Dr. Jiannis Ragoussis, and Mr. Yu Chang at the McGill Genome centre provided the library preparation and sequencing for the 10x scRNa-seq data. Dr. François Mercier provided support and teaching throughout the data analysis stage. Ryan Rys prepared PBMC and tissue samples for bulk TCR sequencing. Samantha Worme for initial data processing. Dr. Piccirillo and, Tho-Alfakar Al-Aubodah provided support and teaching to interpret the T cell scRNA-seq gene expression data.

Discussion: This chapter was written entirely by Matthew Salaciak.

Conclusion: This chapter was written entirely by Matthew Salaciak.

1. Introduction

1.1. Overview of Hodgkin Lymphoma

In the United States, 6% of all diagnosed lymphomas are Hodgkin Lymphoma (HL). Although HL is less common than non-Hodgkin Lymphoma, it is one of the cancers that most frequently affects young adults between the ages of 15-35[1,2]. HL is unique in that malignant cells represent 1% of cells within the tumor microenvironment (TME) which is mostly comprised of benign lymphoid and myeloid cells[3]. HL can be further subdivided into two main classes: classical Hodgkin Lymphoma (cHL), and Nodular Lymphocyte Predominant (NLPHL)[4]. The distinction between classes depends on the type of malignant cell present in the TME; Hodgkin and Reed-Sternberg (HRS) cells or lymphocyte predominant (LP) cells. cHL is the most common class of HL (90%) and will be the focus of this thesis[2]. cHL is curable in 80-90% of patients with chemotherapy, most commonly doxorubicin, bleomycin, vinblastine and dacarbazine (ABVD)[2,5]. During relapse, young and fit patients are offered salvage chemotherapy and autologous stem cell transplant (ASCT), which can lead to long term remissions in ~50% of patients[2,5]. In patients experiencing relapse post-ASCT, or who are deemed ineligible for transplant, immunotherapy with Program Death (PD-1) inhibitors like pembrolizumab is the preferred approach. Success with pembrolizumab is thought to be related to the PD-1/PD-L1 axis which play a key a role in how malignant HRS cells escape immune surveillance in cHL patients[6,7]. While the survival of patients with HL has improved over the years with these therapies, some patients still succumb to the disease. A better understanding of immune activation that occurs in the context of exposure to PD-1 inhibitors, as well as mechanisms of immune exhaustion at relapse, may identify novel targets of immunotherapy for high-risk HL.

1.2. Diagnosis and staging

cHL typically presents with painless enlarged lymph nodes and may be accompanied by fevers, night sweats, and/or unexplained weight loss, otherwise known as “B” symptoms. The diagnosis is established by excisional or core needle biopsy of the involved lymph node(s) or tissue. The presence of HRS cells that express CD30+, CD15+, CD45-, BOB.1- and OCT2- confirms cHL[8]. These cells are derived from germinal center B cells with mutations to the immunoglobulin variable chain gene [3,9,10]. There are four subtypes of cHL: Nodular Sclerosis classic Hodgkin Lymphoma (NSCHL), Lymphocyte-rich classic Hodgkin Lymphoma (LRCHL), mixed cellularity classic Hodgkin Lymphoma (MCCHL), and Lymphocyte-depleted classic

Hodgkin Lymphoma (LDCHL) with NSCHL being the most common subtype[11]. NSCHL involved lymph nodes have a thickened capsule and a visible nodularity formed by fibrotic collagen bands. Within these nodules, HRS cells are found in a background of small lymphocytes, histiocytes and eosinophils[12]. LRCHL presents with a background rich in lymphocytes among vaguely noticeable germinal centers of previously active follicles as well as HRS cells which are identified in the mantle zone[12]. Conversely, the rarest subtype, LDCHL, presents with an increase of HRS cells within a background depleted of lymphocytes in a diffuse fibrotic pattern[11,12]. The HRS cells within MCCHL are dispersed across a background containing eosinophils, plasma cells, neutrophils, small lymphocytes and histiocytes[2]. Sometimes there is minimal effacement of the lymph node architecture leading to HRS cells forming a interfollicular pattern as oppose to a loosely nodular one[12]. Taken together, in all subtypes, ~99% of the lymph node biopsy represents normal immune cells from the TME. It is therefore important to consider how different immune cell infiltrates by subtype may impact the interaction between the TME and HRS cells.

Treatment for HL depends on the stage, which is determined using the Ann Arbor system and based on the presence of disease detected on a positron emission tomography (PET) or computed tomography (CT) scan. Updates to the Ann Arbor staging system by Cotswold also include the extent of extra-nodal extension and tumour bulk (Table 1.1)[13].

Table 1.1 Ann Arbor staging system.

Stage	Description
I	Involvement of a single lymph node region or localized extra-nodal extension.
II	Involvement of two or more lymph node regions on the same diaphragm side or extra-nodal extension with involvement of lymph node regions on the same diaphragm side.
III	Involvement of a two or more lymph node regions or localized extra-nodal extension on both diaphragm sides.
IV	Diffused or disseminated involvement of one or more extra-nodal sites with or without involvement of adjacent lymph node regions.
A	Asymptomatic.
B	Fevers, night sweats and/or unexplained weight loss.

E	Extra-nodal extension.
X	Bulky mass greater than 10 cm.

1.3. Primary treatment

Primary treatment of cHL involves chemotherapy with or without radiation therapy. The recommendation for primary treatment depends on condensing the disease stages into three staging categories: early-stage favourable, early-stage unfavourable and advance stage. Treatment for early stage consists of chemotherapy (3 to 6 cycles), combined modality therapy (2-4 cycles of chemotherapy followed by involved field radiation), or PET-adapted therapy, where the duration of therapy is determined by measuring response after 2-3 cycles of chemotherapy. The most common chemotherapy regimen used in North America is ABVD[5]. [5,14,15]. Advanced disease (stage III or IV) can be treated with 6 cycles of ABVD with a PET-adapted approach being the preferred option, where bleomycin is omitted if the PET scan is negative after 2 cycles.[16,17]. BEACOPP (bleomycin, etoposide, doxorubicin, cyclophosphamide, vincristine, procarbazine and prednisone) and AAVD (brentuximab vedotin, doxorubicin, vinblastine, and dacarbazine) are also suitable regimens for advanced stage HL, with the latter demonstrating a possible survival advantage over ABVD[18]. Currently, there are no PD-1 inhibitors used in the first line therapy of HL outside the context of clinical trials.

1.4. Treatment at relapse

Treatments for cHL achieve sustained remission in >60% of patients, even in the advanced stage setting. The treatment options of patients who experience a relapse depend on the patient's age and co-morbidities[2,19]. ASCT is the standard of care for young and fit patients. Treatment options for disease recurrence after ASCT are limited to immunotherapy therapies like BV and immune checkpoint inhibitors (ICIs) such as nivolumab and pembrolizumab.

1.5. Autologous stem cell transplant

Patients who are young and without significant co-morbidities are offered potentially curative therapy consisting of salvage chemotherapy followed by ASCT in patients who have chemo-sensitive disease[2,5]. Second line chemotherapy referred to as salvage chemotherapy in this setting is used to control the disease and to establish chemo-sensitivity. Patients achieving a partial response or complete response to 2-4 cycles of second line therapy are offered high dose chemotherapy like carmustine, etoposide, cytarabine, and melphalan (BEAM), followed by stem

cell rescue, as this has been demonstrated to be superior to chemotherapy alone and remains the standard of care[2,20]. There are many second line regimens available but the most popular in Canada are gemcitabine, dexamethasone, and cisplatin (GDP) since they are similar in efficacy but have a lower toxicity than other chemotherapy regimens like DHAP [2,5,21]. Although high-dose chemotherapy and ASCT cures about 50% of patients, it is accompanied by an increased risk of treatment-related mortality and long-term toxicities, such as infertility, and development of secondary neoplasms[2,5,22].

1.6. Brentuximab vedotin

Brentuximab vedotin (BV) is an anti-CD30 conjugate composed of molecules of monomethyl aurostatin E, a microtubule disrupter. Once bound to CD30, it is internalized through endocytosis and released into intracellular space. It functions by disrupting the microtubule network within HRS cells leading to G2/M phase cell cycle arrest and apoptosis[23]. In a phase II study of patients who relapsed post ASCT, results show an overall response rate of 75%, a complete response rate of 34%, and within that subset, a 5-year PFS of 52%[24]. The impressive results indicate that BV has curative potential in patients who have recurrent or refractory cHL after ASCT. Additionally, BV can be used as consolidation post ASCT and is also approved in the front line setting within Brentuximab vedotin, doxorubicin, vinblastine, and dacarbazine (AAVD) [25,26].

1.7. Immune checkpoint inhibitors

Although BV provides a promising treatment option for relapse post ASCT, the response rate is still limited. The need to develop additional treatments has led to exciting possibilities within ICIs such as PD-1 inhibitors. One of the immune evasion mechanisms that HRS cells employ is the over expression of PD-L1. The PD-1/PD-L1 axis is a pathway that supresses T cell function to a state defined as exhausted, which is discussed in greater detail in section 2.3. PD-1 inhibitors like nivolumab and pembrolizumab block the PD-1/PD-L1 pathway and has shown to reinvigorate T cells from their exhausted state[2,6,27]. In the relapse post BV setting, PD-1 inhibitors have shown encouraging results with a complete response of ~20% and an objective response rate of 70%[28,29]. Recently, a study compared BV to PD-1 inhibitor pembrolizumab for use in relapse post ASCT and demonstrated a superior progression free survival (PFS) in those treated with pembrolizumab[30]. Despite encouraging results, there is still a need to understand non-responders and immune related adverse events (IRAEs) such as myocarditis and collitis[31].

This has prompted our current research into understanding the immunoregulatory functions within the TME of cHL amongst many cancers.

2 Tumor immunology

HL is a great model to study tumor immunology. From a TME perspective, HRS cells are uniquely able to escape immune surveillance, despite being grossly outnumbered by surrounding immune cells. Furthermore, while 20% of patients with relapsed HL have complete and durable responses to PD-1 inhibitors, 50% of patients have partial and short responses and another 30% fail to respond to these agents at all. The mechanisms of resistance and response to PD-1 inhibitors in HL are poorly understood. New knowledge of immune evasion beyond the PD-1/PDL-1 axis is needed, which may reveal therapeutic targets that can benefit the 80% of patients not cured with these drugs.

In this chapter, I will highlight the important components of the immune system, then contrast healthy immune responses to dysfunctional responses as seen in the context of cancer or chronic infections. I will start by comparing innate and adaptive immunity, humoral, and cell mediated immunity, as well as highlight the important role of antigen presenting cells. I will contrast this to what is known about the HL TME, focussing on the important relationship between HRS cells and surrounding immune cells, especially T cells. Finally, I will review concepts of immune exhaustion, including T cell subsets that may be important in controlling tumor growth.

2.1 Cellular components of an effective immune response

The innate immune response is characterized by its immediate induction and antigen independence[32,33]. Cells involved in innate immunity quickly recruit immune cells to areas of infection and inflammation by producing cytokines and chemokines. These cells include myeloid cells such as macrophages, dendritic cells, neutrophils, mast cells, eosinophils, basophils, and lymphoid cells like Natural Killer (NK) cells[33,34]. NK cells are similar to T cells in that they are both highly cytotoxic, however NK cells are considered innate lymphoid cells because they do not require antigen presentation[33,35].

Lymphoid derived cells, such as B and T cells do in fact require antigen presentation and are key to the adaptive immune response[32,36]. Adaptative immunity is antigen dependent and antigen specific, meaning that B and T cells have great specificity for their respective target antigen. Adaptive immunity is a slower process that results in immunologic memory and thus the

capability to recognize the same target antigen if re-exposed[33]. The innate and adaptive immune systems are complementary systems, with the adaptive system requiring activation by an innate immune response. A typical example of this is when a phagocytic cell such as a macrophage presents an ingested antigen to T cells. Antigen presenting cells (APCs), like macrophages and dendritic cells, are important because they initiate the adaptive immune response. APCs secrete chemokines and present tumor antigens on their MHC class II receptors which recruit and activate T cells[32,37]. (Figure 2.1).

The adaptive immune response can be divided into two main groups: humoral, which is B cell-mediated and cellular, which is T cell-mediated. B cells kill extracellular microbes such as bacteria and can produce antibodies. Secreted antibodies bind to antigens on the surface of pathogens which flags them for destruction, ultimately preventing entry into normal cells. B cell antigen recognition is through their B cell receptor (BCR)[38]. For B cells to produce antibodies, they require activating signals from helper T cells. B cells will present processed antigens on MHC class II molecules to antigen specific helper T cells to start this process[38]. In cell mediated adaptive immunity, antigen specific T cells effectively eliminate microbes or virus infected cells as well as cancer cells. Cytotoxic T cells will target virus-infected cells, cells with intracellular bacteria and cancer cells since they will all present foreign antigen through their respective MHC class I molecules[34,38,39]. As previously mentioned, helper and cytotoxic T cells recognize antigens presented on either MHC class I or MHC class II molecules. This restriction is functionally important and will be discussed in the next section.

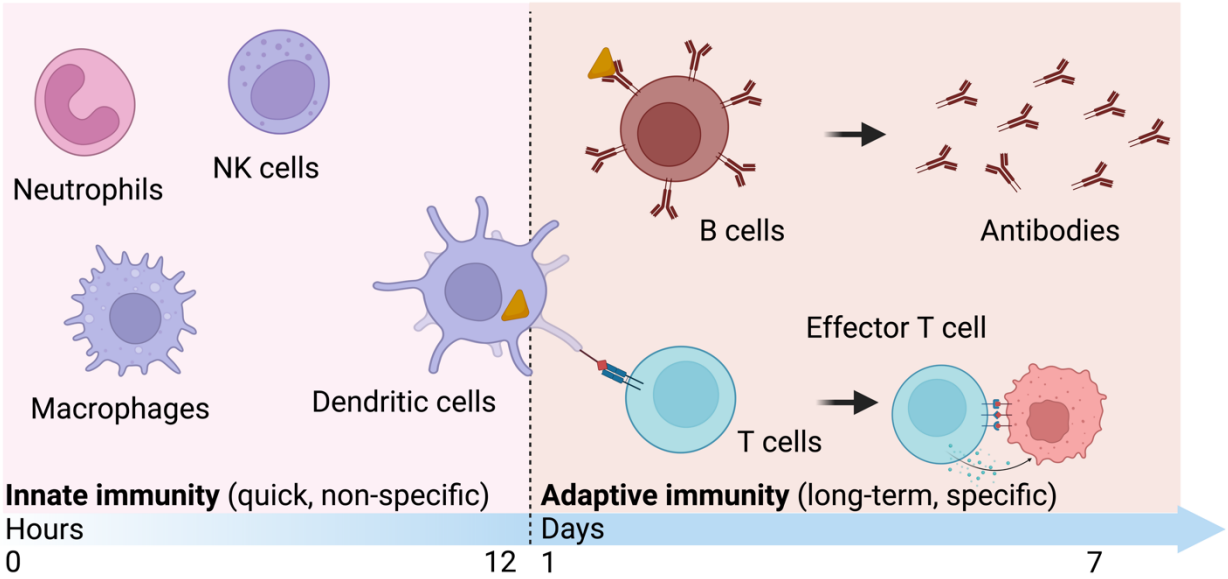

Figure 2.1 Innate and adaptive immune system. Overview of the innate and adaptive immune system highlighting key cellular components and response timeline. This figure was adapted from *Cellular and Molecular Immunology by Abul K. Abbas*[40].

2.2 Normal T cell function and activation

CD4+ and CD8+ T cells play a critical role in tumor suppression. Nomenclature and function of T cells is determined by expression of either CD4 or CD8 receptors. CD4+ T cells referred to as T-helper cells recognize MHC class II antigens and mediate the adaptive immune response by producing pro-inflammatory cytokines and activation signals for B cells. CD4+ T cells have multiple effector subsets known as Th1, Th2, Th9, Th17, Th22 and Tfh. Each subset has different functions and produces a variety of cytokines that ultimately distinguish one another[41]. CD4+ Treg cells are a specialized subset that have immunosuppressive functions to mediate immune self-tolerance.[42] CD8+ T cells, also referred to as cytotoxic or killer T cells, target abnormal or virus/pathogen infected cells by recognizing MHC class I antigens. Once a T cell is activated, it differentiates from a naïve T cell into various effector and memory subsets. T cell activation begins when APCs activate naïve T cells expressing cognate T cell receptors (TCRs) and co-stimulatory receptor CD28 via B7-1 and B7-2 co-stimulatory ligands and antigens loaded on MHC molecules[43]. Once activated, T cells proliferate and differentiate in response to pathogenic or tumorigenic stimuli. During T cell expansion, naïve T cells produce IL-2, IL-4, and IL-7 cytokines to increase survival and proliferation[43,44]. Expansion of T cells ceases once stimuli has been cleared and/or CD4+ Tregs have intervened to limit expansion. At this point, the expanded T cells contract and die with a small fraction remaining as memory T cells. Memory T cells exist in greater numbers than naïve T cells that bear the same TCR, allowing for a more rapid response to proliferate upon antigen re-encounter. Memory T cells are quite heterogenous and can be classified as memory stem T cells (Tscm), central memory T cells (Tcm), effector memory T cells (Tem), and tissue resident memory T cells (Trm), based on their metabolic, transcriptional, and epigenetic states[44,45]. Studies support a progression model of memory T cell differentiation starting from naïve T cells, to Tscm, Tcm, Tem, and eventually ending in a terminal effector subtype (Tte) (Figure 2.2)[45–47]. In the case of TCR re-engagement there are different T cell fates to maintain immune homeostasis. In acute strong restimulation, restimulation-induced cell death, an apoptotic pathway, is trigged[48].

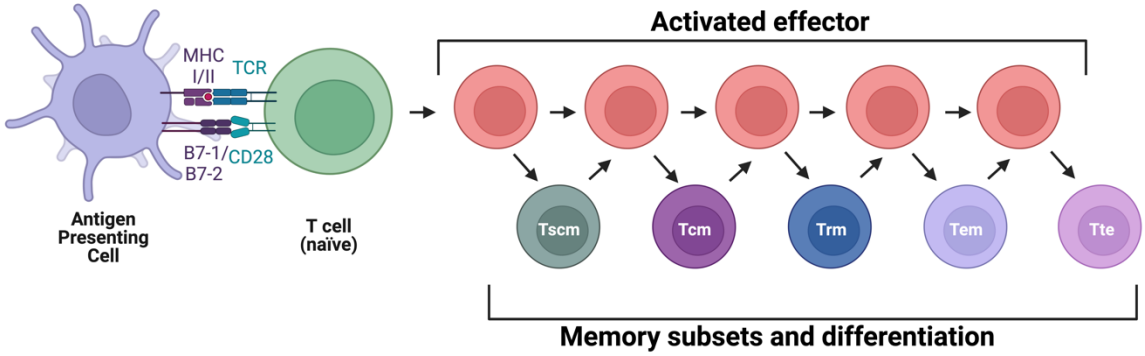

Figure 2.2 Differentiation process of a T cell. Once primed from an APC, a T cell will become an activated effector and expand. Expansion will cease once primary response or infection is terminated and some effector cells differentiate into various memory subsets. Upon exposure to the same antigen, the memory T cell will once again become an activated effector, following the previous cycle until reaching a terminal state. This figure was adapted from Mahnke et *al*[47].

2.3 T cell exhaustion

In the context of chronic weak antigen stimulation, T cells that exhibit features of decreased effector function are considered to be exhausted. CD8+ effector T cells undergo phenotypic and functional changes promoting an exhausted state in response to chronic antigen stimulation from persisting infections or tumors, resulting in decreased cytotoxicity and an increase in inhibitory receptors such as PD-1, LAG-3, CD244 (encodes protein 2B4), and HAVCR2 (encodes protein TIM3)[49–51]. CD8+ T cell exhaustion has been the focal point of immunotherapy in cancers with the advent of ICIs, especially PD-1 inhibitors. Although there exists heterogeneity within exhausted T cells, recent studies have elucidated the existence of at least two distinct subsets of exhausted T cells: precursor exhausted (Tpex) and terminal exhausted (Tex)[50] (Figure 2.3). There are notable differences between Tpex and Tex cells in terms of expression of inhibitory receptors, surface molecules, cytokines, chemokines, cytotoxic molecules, and transcription factors. Interestingly, Tpex T cells share similarities to memory T cells while possessing the ability of self-renewal by expressing transcription factor TCF1 (encoded by *TCF7*) amongst others, which makes them almost "stem memory like"[50]. In contrast, Tex T cells are terminally differentiated and cannot self-renew. Besides giving rise to terminally exhausted T cells, studies have suggested that the precursor exhausted subset are responsible for the proliferative burst and increased effector function after immunotherapy treatment such as PD-1 inhibitors[44,50,52,53]. The concept of precursor exhaustion has provided a

change in perspective and a new framework to investigate immune exhaustion in the context of cancer and immunotherapy treatments.

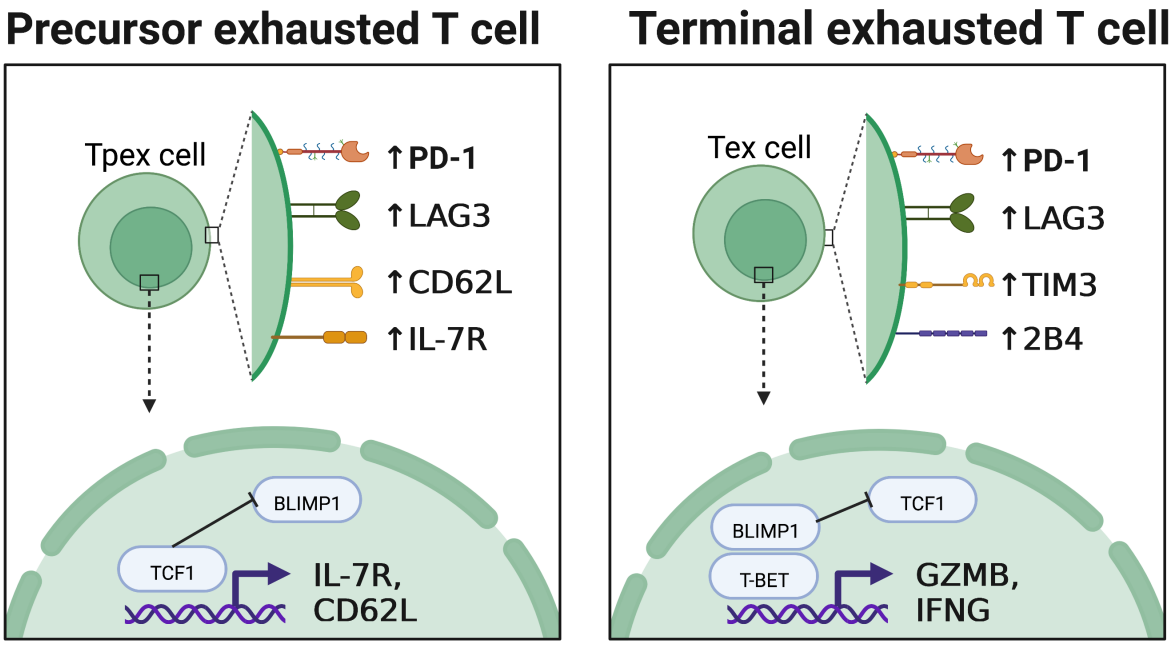

Figure 2.3 Precursor and terminal exhausted T cell expression differences. Key differences in exhaustion markers and transcription factors between Tpex and Tex cells. Tpex cells express markers associated to memory and self-renewal such as CD62L, IL7-R and TCF1 (encoded by TCF7). Tex cells express multiple exhaustion markers as well as BLIMP-1 (encoded by *PRDM1*) and T-BET (encoded by *TBX21*) which contribute to a highly cytotoxic terminal state and inhibit TCF1 expression. This figure was adapted from *Precursor exhausted T cells: key to successful immunotherapy by Kallies et al.*[50]

Table 2.1 T cell subsets.

Subset	Phenotype	Function	References
Tscm	$CD62L^{hi}$, $CCR7^{hi}$, IL7RA, CD45RA	Antigen experienced. Capable of self-renewal and reconstitution of all memory T cells.	[44–46]
Tcm	$CD62L^{hi}$, $CCR7^{hi}$	High expression of lymph node homing molecules, limited effector function.	[44–46]

Tem	CD62L^{lo}, CCR7^{lo}	Rapid effector function, traffic to inflamed tissues.	[44–46]
Trm	CD103^{hi}, CD69^{hi}	Does not circulate, stays retained in tissue.	[44–46]
Tpex	IL7RA, CD62L, PDCD1, LAG3, TCF1, GZMK	Self-renewing precursor exhausted T cell. Limited effector and cytotoxic capacity but have potential for proliferation.	[44,50,54,55]
Tex	PDCD1, LAG3, HAVCR2, 2B4, BLIMP1, TBET, GZMB	Terminally differentiated exhausted T cell. Limited effector, cytotoxic and proliferative capacity.	[44,49,50]

2.4 Hodgkin Lymphoma: HRS cells, the master regulators of the TME

In HL, HRS cells are genetically programmed to thrive and escape immune surveillance despite being surrounded by a rich inflammatory infiltrate[2,11] (Figure 2.4). Genetic profiling has shown that their survival and growth is mainly ensured by consistent activation of nuclear factor kappa B (NF-kb), janus kinase signal transducer and activator of transcription (JAK/STAT) signalling, and TME crosstalk. Studies have found that gain/amplification mutations which result in the overexpression of the *REL* gene, as well as gain and structural changes to the loci of *BCL3* and *MAP3K14*, all contribute to NF-kb pathway activation[56–58]. *REL* overexpression has been documented in 70% of cHL cases[58]. Mutations affecting inhibitors such as *NFKBIA*, *NFKBIE*, *TNFAIP3* also contribute to NF-kb pathway activity[59,60]. In cHL, the JAK-STAT pathway is consistently activated either through autocrine and paracrine signaling or dysregulation of the JAK-STAT pathway which one study has demonstrated in 87% of cases through whole genome sequencing of micro-dissected tumor samples[61]. In cHL, the common amplification of 9p24.1

leading to overexpression of *JAK2*, mutations coupled with inactivating negative JAK-STAT regulators such as *SOCS1* contribute to the persistent JAK-STAT activation[57,62,63].

The formation of the TME is mainly orchestrated by chemokines and cytokines produced directly from HRS cells or from their inducive effect on infiltrates. A hallmark of cHL's TME is the abundance of CD4+ T cells. Additionally, HRS cells recruit monocytes, eosinophils, macrophages, plasma cells, fibroblasts, and NK cells through chemokines. The curated milieu has been carefully studied to yield greater insight into the symbiotic relationship between HRS cells and the TME. Studies have shown that CD4+ T cell subsets contribute a myriad of cytokines implicated in the TME crosstalk. For example, CD4+ Th2 cells have an important role in cellular crosstalk through a production of a large variety of cytokines that contribute to proinflammation, infiltrate recruitment and immunosuppression[8,58,64,65].

It has also been demonstrated that HRS cells have reduced expression of MHC class II and I receptors on their surfaces and identified genetic lesions contributing to increased PD-L1 expression. This allows HRS cells to avoid T cell-mediated cell death and promote T cell exhaustion through the PD-1/PD-LI axis. Additionally, HRS cells regulate the TME by recruiting infiltrates such as CD4+ Tregs to induce an immunosuppressive environment.

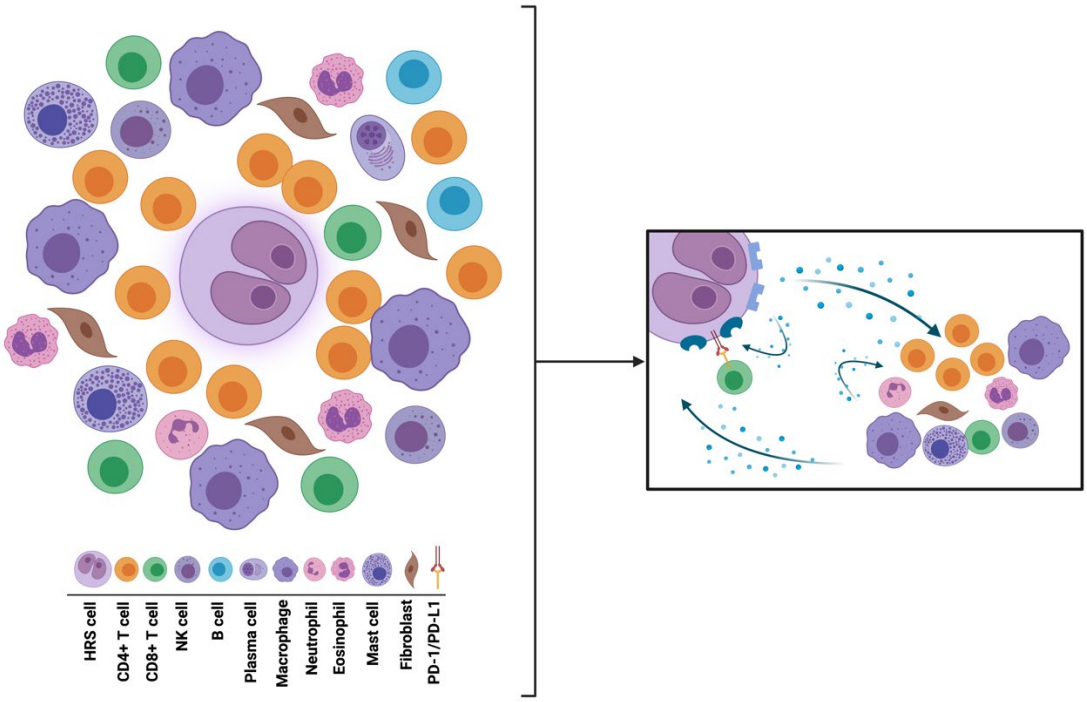

Figure 2.4 Overview of the TME in cHL. The HRS cell is encapsulated within a highly inflammatory background that consists of multiple immune cells. The smaller box provides a snapshot into the complex cross talk within the TME. The growth of HRS cells as well as their ability to avoid immune surveillance by taking advantage of multiple immune escape mechanisms such as the PD-1/PD-L1 axis is dependent on this carefully curated TME.

2.5 T Cells within the TME

T cells are the most characterized and likely the most important immune cells in the TME. Common between all subtypes is the dominance of CD4+ T cells, often spatially found forming rosettes around HRS cells[66]. In cHL, multiple studies have identified CD4+ T cell clusters to be mainly effector Th2 and regulatory Treg subtypes[67,68]. Recent studies focusing on the heterogeneity of CD4+ T cells have found that CD4+ Th1 cells are more frequent compared to Th2 cells than previously thought. [69,70]. The use of single-cell RNA sequencing (scRNA-seq), immunohistochemical (IHC), imaging mass cytometry (IMC) and CyTOF techniques have provided further insight into the TME. Recently, studies employing such techniques have identified phenotypically distinct T cell subsets within the TME such as a immunosuppressive Tr1 CD4+ LAG3+ population that were enriched in MHC-II negative HRS cell cases as well as an expansion of Th1 with intermediate to high expression of PD-1 inhibitory receptor [69,71]. The

detailed analysis of such CD4+ T cell subsets have shown to be instrumental in curating a pro-inflammatory and immunosuppressive TME that contributes to HRS cell survival. CD8+ T cells are less frequent in the TME compared to CD4+ T cells[72]. Despite their infrequency, CD8+ T cell subtypes within the TME have been identified as effector memory and terminally differentiated effector memory CD45RA+ subsets [45,69]. This has led more research exploring the landscape of cHL tumor infiltrating T cells within the TME. Researchers using bioinformatic approaches from scRNA-seq data have revealed unique phenotypic subsets of T cells expressing inhibitory receptors such as PD-1,CTLA-4 and LAG-3 that contribute to T cell exhaustion[73,74]. This has implications into how HRS cells employ immune evasion and immunosuppression mechanisms which will be discussed in the subsequent section.

2.6 Mechanisms of immune evasion, immunosuppression, T cell exhaustion in HL

2.6.1 Immune evasion

The TME of cHL demonstrates how HRS cells recruit infiltrates to take advantage of the induced cellular crosstalk that promotes their growth and survival via signaling pathways. Interestingly, to ensure unchallenged growth and survival, HRS cells secrete immunosuppressive cytokines such as IL-10, TGFb and *EBI3* while employing immune evasion mechanisms. HRS remarkably educate normal cells to promote an immunosuppressive environment while exploiting intrinsic modifications to evade antigen-dependent immune responses. HRS cells can have a complete loss or severe reduction of MHC class I and/or Class II, affecting CD8+ T cell effector response and antigen presentation to CD4+ helper T cells. Inactivating mutations and/or deletions of B2M is the most common cause of aberrant MHC class I expression in 79% of cHL cases[75–77]. Similarly, inactivating mutations and/or deletions of *CIITA* result in reduced or loss expression of MHC class II in ~40% of cHL cases[78,79].

2.6.2 HRS cells can induce an immunosuppressive TME

HRS cells uniquely educate the recruited cellular milieu to curate an immunosuppressive environment. HRS cells induce polarization of CD4+ T helper cells to a Treg phenotype as well as monocytes to M2 tumor-associated macrophages (TAMs), which promote an immunosuppressive environment. CD4+ Tregs marked by the expression of CD25, CTLA-4, CD39, FOXP3 and production of IL-10 are found in abundance within the TME[42,67]. To further investigate this mechanism, one study cocultured bulk CD4+ and CD4+ CD25- T cells from healthy donors with HRS cells. It was shown that both CD4+ T cell populations produced Treg

subpopulations[80]. Interestingly, the study repeated the same experimental parameters but cocultured with DLBCL lines and found no increased Treg populations establishing Treg induction a potentially unique feature of cHL. CD163+ M2 macrophages are immunosuppressive, blunting immune responses by producing large amount of IL-10[81]. In cHL, it has been demonstrated that M2 TAMs are associated with a poor prognosis which prompt research into the polarization of monocytes into M2 TAMs within the TME[82,83]. Multiple studies coculturing either monocytes or M1/M2 macrophages with cHL condition medium have shown the ability of HRS cells to polarize monocytes to M2 TAMs[82,84]. In the TME, growth factors M-CSF and GM-CSF and cytokines IL-4, IL-10 and IL-13 are present and known to induce polarization to M2 TAMs, which eludes to the importance of cellular crosstalk within the TME for HRS survival[81–83].

2.6.3 T cell exhaustion

HRS cells further evade an immune response by inducing a state of T cell exhaustion through the secretion of ligand PD-L1/L2 which provides constant activation of the PD-1 receptor on T cells[85]. Remarkably, HRS cells are genetically programmed to overexpress PD-L1 and PD-L2 through amplification of 9p24.1. This also includes *JAK2*, leading to an over expression of *JAK2* which also promotes expression of PD-L1 through JAK-STAT signalling[75,86]. Additionally LMP1 expression in Epstein-Barr virus involved cases further induces over expression of PD-L1 in HRS cells from signaling the JAK-STAT and AP-1 pathways[87]. Recently, a topological analysis of cHL revealed that the majority of PD-L1 expression in the TME is through PD-L1+ TAMs[88]. Furthermore, the same group showed that there is a niche within the TME of PD-1+ CD4+ and CD8+ T cells surrounding HRS cells with CD4+ T cells in closer contact to HRS cells than CD8+ cells. Within this niche it was noted that PD-L1+ TAMs were closer to HRS cells than PD-L1- TAMs suggesting a highly organized immunosuppressive TME[88].

2.7 Therapeutic targets

In HL, PD-1 inhibitors have shown high response rates but there is little known about the biomarkers of response and resistance. HRS cells with amplification of 9p24.1 and expression of MHC class II receptors is associated with a favourable response, however biomarkers of resistance other than LAG-3 have not yet been explored in HL[89,90]. Recently, it has been shown that the proliferative burst and T cell effector activity after PD-1 inhibitor treatment may be

coming from Tpex cells. Tpex cells have the capacity for self-renewal allowing for the generation of effector and memory phenotype cells on antigen re-exposure. In contrast, Tex cells do not possess this ability which may be why they fail to respond to PD-1 inhibitors[50,53,55,91]. This implies the presence of Tpex cells may have potential to be used as a biomarker of response.

Currently, the field has been focused on expanding possible response and resistance biomarkers. One group has identified a peripheral immune signature associated with responsiveness in cHL patients. By using TCR sequencing coupled with cytometry by time-of-flight they show that PD-1 inhibitors was most effective in patients with a diverse TCR repertoire pre-treatment, resulting in an expansion of singleton clones, an increase in CD4+ TCR diversity and an abundance of activated NK cells[73]. This study highlights an interesting deviation shifting focus from CD8+ effector T cells to other immune cells. Current exploration of mechanisms of resistance has led groups to characterize the heterogeneity within exhausted T cells aiming to isolate subsets that respond to ICIs. The transcriptome of tumor-infiltrating CD8+ T cells from melanoma and non-small cell lung cancer (NSCLC) samples were analyzed using scRNA-seq[92]. This group showed that higher expression of transcription factor Tox was associated with more exhausted T cells and worse overall survival in melanoma and NSCLC. Additionally, they demonstrated that in TOX knockout models, CD8+ T cells had downregulation of inhibitory receptors of PD-1, TIM-3, TIGIT and CTLA-4[92].

Other groups have also identified a critical role of TOX as a regulator of T cell exhaustion, demonstrating the value in investigating mechanisms of T cell exhaustion[93,94]. Going beyond PD-1 inhibition, researchers have been focusing on other immune checkpoint targets that could be involved in intra-tumoral T cell exhaustion. Furthering our understanding of T cell exhaustion, the identification and characterization of new immune checkpoints are becoming increasingly important with large emphasis of potential blockade targets. Three inhibitory checkpoints, LAG-3, TIM-3 and TIGIT as shown in Table 2.3 have had increase focus to understand their involvement in T cell exhaustion. Interestingly, there has been evidence that LAG-3 and TIM-3 are expressed in 98% and 96% of samples in a cohort of 57 cHL cases respesctively[95]. TIGIT was expressed almost exclusively on PD-1+ T cells in 86% of cHL cases from a cohort of 40[96].

Beyond biomarkers of response and resistance, there is a growing body of research to identify biomarkers of iRAEs. The identification of such markers will help predict potentially severe iRAEs and aid in clinical decision making. Currently, there is no single biomarker that has proven to be predicative, however groups have provided multiple avenues to explore. Recent studies have shown increased IL-6, TNFα, IFNα and C-reactive protein (CRP) to be associated with iRAEs[97–99]. Additionally, high neutrophil to lymphocyte ratio, increase of white blood counts with decreased relative lymphocyte counts have been associated to iRAEs[97,98]. Taken together, these findings highlight the need to investigate biomarkers into response, resistance and iRAEs as well as identification of potential immune checkpoints.

Table 2.2. Inhibitory receptors

Inhibitory checkpoints	Expression	Signalling and Inhibition	References
LAG-3	CD4+ and CD8+ T cells, NK cells, dendritic cells, and B cells.	High affinity for MHC class II, inhibitory role on T cell immune response and T cell memory activation.	[100]
TIM-3	Mainly CD4+ Th1 T cells, CD4+ and CD8+ T cells.	Evidence of co-expression and cooperative with PD-1	[101]
TIGIT	CD4+ and CD8+ T cells, and NK cells.	Main ligand CD155 is expressed on dendritic cells, B cells and macrophages, inhibits T cell effector function	[102]

2.8 Single-cell RNA sequencing in immuno-oncology

Being able to interrogate gene expression at the single-cell resolution has been a crucial tool in medical research and clinical practice/diagnostics. However, instruments used for this application like flow cytometry and mass cytometry by time of flight are limited to measuring about 20 and 40 markers respectively[103,104]. To further characterize cellular heterogeneity,

identify gene expression programs, and infer deeper biological understanding of disease, scRNA-seq has provided a transformative way to explore entire transcriptomes at the single-cell resolution. scRNA-seq generates large amounts of data that fortunately is accompanied by a rapid development of analytical tools. Analytical methods such as cellular fate mapping, chromatin accessibility, immune profiling, and gene co-expression analysis have provided and will continue to provide profound biological insight.

2.8.1 Overview of scRNA-seq

Since the first single-cell mRNA was sequenced in 2009, there has been ample advancement in sequencing technologies along with a variety of protocols[105]. In essence, all the protocols follow a general schematic consisting of single-cell capture, cell lysis, reverse transcription, and amplification that concludes library preparation prior to being sequenced[106]. 10x genomics is one of the most common scRNA-seq platforms that uses a droplet-based microfluidics method. This protocol consists of on-bead primers with barcodes to identify individual cells and uses unique molecular identifiers (UMIs) to quantify gene expression per cell[107]. The primers contain a polydT sequence that binds to the polyadenylated mRNA at the 3' end for reverse transcription[107]. As a result, only the 3' end is sequenced which can be a limitation. Currently, new experiments requiring a multiomic approach have been a catalyst for developing new scRNA-seq protocols and computational tools. Immune profiling, a commonly used multiomic approach provides the ability to capture the transcriptome alongside the full-length V(D)J sequences for B cell and T cell receptors (BCRs/TCRs). V(D)J transcripts are located within the first 500 nucleotides at the 5' end, which requires an adaptation from the current protocol to overcome the 3' limitation[108]. To achieve this, the polyDT sequence is supplied as a reverse transcription primer instead of being included in the bead like the 3' protocol.

2.8.2 Immune profiling applications

The ability to profile the entire transcriptome and paired BCRs/TCRs simultaneously at the single-cell resolution has provided researchers a crucial tool in immunology and immuno-oncology research. Countless studies have utilized these methods to explore immunotherapy response and resistance mechanisms, revealing cellular states within a heterogenous immune response to disease and to provide immune cell scRNA-seq atlases. Transcriptome data at this resolution requires advanced computational analysis to derive

meaningful information and insights. Clustering algorithms are crucial in grouping together thousands of individual cells into clusters that share similar expression profiles, allowing us to infer what cells are present in our sample. Additionally, studies have employed weighted gene co-expression network analysis to identify sets of correlated genes. Moreso, techniques to assess the expression of these sets have been useful in identifying gene programs within heterogenous populations. In the context of immunotherapy scRNA-seq research, coupling TCR data with identified correlated genes (which can be referred to as gene sets, transcriptomic signatures, or gene signatures) can provide powerful insights. Studies have demonstrated which T cells or T cell clusters are tumor derived and/or involved in therapeutic responses while assessing identified associated gene sets[109–111]. Table 2.4 is a non-exhaustive list highlighting pivotal studies that utilize scRNA-seq immune profiling methods.

Table 2.3. Summary of pivotal studies using scRNA-seq immune profiling methods.

Authors	Summary
Sade-Feldman et al. (2018)[112]	scRNA-seq immune profiling revealed a transcription factor, TCF7+ (encodes TCF1), T cell subpopulation that is associated with positive outcome in response to immunotherapy in melanoma.
Guo et al. (2018)[113]	scRNA-seq immune profiling of T cells from 14 treatment naïve non-small-cell lung cancer patients described a heterogenous T cell landscape comprised of differing ratio of pre-exhausted to exhausted T cells along with Tregs expressing an activation marker, TNFRSF9, that correlate to better prognosis or worse prognosis respectively.
Yost et al. (2019)[114]	scRNA-seq immune profiling of matched tumors before and after PD-1 blockade therapy. Tracked TCRs and transcriptional phenotypes showed that expansion of T cell clones did not derive from pre-existing tumor-infiltrating lymphocytes. Expanded clones were found to be from new clonotypes and were preferentially observed in exhausted subsets.
Li et al. (2019)[115]	scRNA-seq and TCR analysis of 25 melanoma patients contributed to the identification of a T cell dysfunction gradient from using weighted co-expression network analysis. Proliferative CD8+ T cells was more profound in early dysfunctional states.

Zhang et al. (2020)[110]	scRNA-seq and TCR analysis immune profiling of non-small-cell lung cancer patients across immunotherapy treatment. They found that circulating tumor related CD4+ T cell clones had higher cytotoxic activity and were in abundance after disease progression.
Zhang et al. (2020)[116]	scRNA-seq immune profiling of PBMCs of 5 healthy donors and 13 COVID-19 patients to determine transcriptional profiles of immune cells in COVID-19. Most immune cells in COVID-19 patients showed a strong overall acute inflammatory response, intensive expansion of cytotoxic T cells in moderate patients and dysfunctional interferon response, immune exhaustion, and skewed TCR repertoire in severe patients.
Corridoni et al. (2020)[117]	scRNA-seq immune profiling to create a single-cell atlas of colonic CD8+ T cells in ulcerative colitis derived from healthy and ulcerative colitis human samples.
Pauken et al. (2021)[118]	scRNA-seq and TCR immune profiling of blood from mice with MC38 tumors or melanoma patients. This study characterized immunotherapy response from circulating CD8+ T cells from joint scRNA-seq and TCR analysis and found NKG2D, CD39 and CX3CR1 to be associated with circulating tumor infiltrating CD8+ T cells.
Liu et al. (2022)[111]	scRNA-seq immune profiling of 47 tumor biopsies from 36 patients with NSCLC reveals a temporal clonal revival and expansion of precursor exhausted T cells during PD-1 blockade therapy. In responsive tumors, an increase of precursor exhausted T cells was observed in contrast to non-responsive tumors that did not accumulate precursor exhausted T cells.
Lozano et al.[119] **(2022)**	scRNA-seq immune profiling combined with mass cytometry by time of flight, bulk RNA and bulk TCR/BCR sequencing of PBMC samples to define T cell phenotypes associated with toxicity to ICIs in patients with melanoma. Two pre-treatment factors associated with serve iRAE were abundance of circulating activated CD4+ memory T cells and large TCR diversity.

2.9 Conclusion

The unique TME of cHL grants us the opportunity to investigate the dynamics of a highly inflamed cancer, with questions stemming from a synergistic relationship between immunology and oncology. The ability of HRS cells to carefully curate the TME to promote its growth and survival while evading an immune response is truly remarkable. Deciphering the immune crosstalk within the TME has led to many insights that have translated into actionable treatments such as PD-1 inhibition. Despite these successes, there are many questions left to further elucidate the immune evasion mechanisms with hopes to improve PD-1 and other immune checkpoint blockades. The increasing use of NGS technologies such as WGS and scRNA-seq is generating vast amounts of data that can be applied to identify clinically useful ICI targets, biomarkers to determine response to ICIs and signaling pathway inhibition targets. Interestingly, studies have indicated that the reinvigoration of exhausted T cells documented by effector T cell generating proliferative burst after ICIs may be derived from Tpex T cell population[50,111]. There is still much to explore and understand about the mechanisms involved with ICIs, especially with regards to cancer type and tumor microenvironment.

3 Hypothesis and objectives

HRS cells orchestrate a complex microenvironment which encourages growth and immune evasion. HRS cells commonly overexpress PD-L1 which exploits the PD-1/PD-L1 immune checkpoint axis, effectively disarming infiltrating T cells. Although immune checkpoint inhibitors such as PD-1 blockade are highly effective in refractory or relapsed cHL, mechanisms of action and resistance remain undefined. It is crucial to have a better understanding of how T cell effector function is re-established or conversely, understand mechanisms of relapse following PD-1 inhibition in patients with cHL. We hypothesize that beyond PD-1, additional features of T cell exhaustion may prevent effective response to PD-1 inhibitors in HL.

Our objectives are to identify the transcriptional changes in immune cells that are associated with disease response and the development of irAE in a cHL patient treated with pembrolizumab. In addition, we will track the clonal dynamics of T cells in the peripheral blood and cHL tumor tissue across time points by linking scRNA-seq data to TCR receptor sequencing data.

We will perform scRNA-seq on the peripheral blood mononuclear cells (PBMCs) across several clinically-important time points: cHL relapse pre-exposure to PD-1inhibitor treatment, complete response during PD-1inhibitor treatment, cHL relapse while off PD-1inhibitor treatment and progressive disease upon PD-1inhibitor re-treatment). Two additional time points are in the context of the onset of pericarditis, the irAE that initially occurred while in remission but also recurred on PD-1inhibitior re-challenge at the time of progressive disease. This profiling may reveal key immunomodulatory effects that will provide insight into mechanisms of action and resistance of PD-1 inhibitors within cHL patients as well as the pathology that occurs in irAE. The overarching goal is to identify biomarkers of response and reveal additional targets for future therapies in patients not responding to PD-1 inhibitors.

To our knowledge, previous studies using single-cell transcriptomics to profile the immune cell landscape of PD-1 inhibitors have been exclusively carried out in solid tumor cancers. This highlights the need for a high-resolution approach to profile the peripheral immune response across PD-1 inhibitor treatment in cHL. By performing scRNA-seq of PBMCs from six treatment time points of five discrete disease: PD-1 inhibitor treatment naïve, remission, relapse, treatment rechallenge, and disease progression from a cHL patient, we aim to characterize the immune cell landscape to provide a comprehensive overview of expression changes across treatment. Our analysis begins by first defining the immune cell subsets found within our PBMCs data, where T cells showed most significant expression and proportion changes. From this, we focused our analysis on T cells, leveraging TCR data that accompanied our scRNA-seq dataset. In addition, we performed bulk TCR sequencing on available PBMC and tumor tissue samples. We then analyzed T cell clones allowing us to characterize and track clonal dynamics across treatment time points within PBMCs and tumor tissue that revealed an underlying heterogeneity in CD8+ T cells. We resolved T cell heterogeneity through definition of two novel signatures related to stem memory or terminal effector like phenotypes through gene co-expression network analysis of CD8+ T cells. Ultimately, we aim to profile the immune cell landscape to provide insight into the functional changes during PD-1 inhibition. This aligns with our labs goal to uncover novel potential biomarkers and therapeutic targets which may lead to improved immunotherapy treatments.

4 Materials and Methods

Sample selection. Our institution has established a large lymphoma cell bank which includes viable cryopreserved PBMCs. Samples are purified using Ficoll gradient centrifugation and cryopreserved at -196°C until recovery. PBMCs of lymphoma patients treated with anti-PD-1 are banked at each treatment time point after patients provided consent. The project is approved by our Research Ethics Board (12-052 and 18-12). We recovered six treatment time point samples of one r/r cHL patient to perform scRNA-seq.

Single-cell RNA-seq library preparation. Frozen samples were sent to the McGill Genome Centre for library preparation and sequencing. Droplet-based scRNA-seq using the Chromium 5' library protocol with simultaneous single cell V(D)J enrichment for human B and T cells was performed. Libraries were sequenced using the Illumina NextSeq 500. We are grateful for our collaboration with Dr. Jiannis Ragoussis, and support from Mr. Yu Chang at the McGill Genome centre.

CyTOF library preparation. Remaining PBMCs were used for CyTOF library preparation. Fluidigm Maxpar Human T cell phenotyping and expansion panels in addition to human T cell immune-oncology expansion panels were used. Markers from all panels include, CCR4, CCR5, CCR7, CD2, CD3, CD4, CD5, CD7, CD8a, CD9, CD11a, CD16, CD25, CD27, CD28, CD44, CD45, CD45RA, CD45RO, CD49d, CD57, CD69, CD95, CD127, CD134, CD137, CD152, CD161, CD223, CD278, CD279, CD336, CXCR3, HLA-DR.

Bulk T cell receptor sequencing library preparation. Three PBMC samples and two formalin-fixed, paraffin embedded (FFPE) needle core tumor tissue biopsy samples were used for bulk TCR sequencing. DNA/RNA was extracted following the AllPrep DNA/RNA protocol from Qiagen. LymphoTrack TRB assay panel from invivoscribe was used to prepare TCR sequencing libraries from genomic DNA. Libraries were sequenced within our institution on an Illummina MiSeq sequencer with aid from Dr. Yury Monczak. Raw FASTQ files were processed using MiXCR to quantify clonotypes[120].

Single-cell RNA sequencing data pre-processing and quality control. scRNA-seq sample reads were trimmed, demultiplex and aligned to the reference genome (cellranger GRCh38/hg19). Unique transcripts were counted using 10x Genomics pipeline cellranger 2.2.0 outputting both filtered and unfiltered count matrices. Quality control of expression matrices was performed in R using Seurat 4.1.0 package[121,122]. Quality control was performed for each sample

prior to being merged. Ambient RNA contamination was assessed and removed using 10X suggested third-party resource SoupX[123]. Doublets were identified using Python programming language along with scrublet and removed within R[124]. Cells in each sample were filtered such that each gene was expressed in at least 3 cells and each cell has a minimum of 200 expressed genes. Mitochondrial gene expression per cell was assessed for each sample. On average, cells expressing more than 11.32% mitochondrial genes were excluded from further downstream analysis. Additionally, cells containing hemoglobin genes and platelets were removed. Each sample was normalized independently by Seurat's normalization method which scales each cell's UMI by 10,000 then performs a log normalization[122].

Merging, dimensionality reduction and clustering. Using Seurat, individual samples were merged to proceed with further downstream analysis. The joint dataset was then subjected to a workflow that consisted of identifying 2000 of the most highly variable genes based on average expression and dispersion, scaling gene expression per sample, principal component analysis (PCA) and dimensionality reduction using UMAP[122,125]. The first 20 principal components (PCs) were used as input for clustering and visualization. Cells were clustered by first constructing a K-nearest Neighbors (KNN) graph and then applying the Louvain algorithm, a modularity optimization technique with a resolution of 0.5[126–128]. Clusters were assigned cell identities based on canonical markers retrieved from Seurat's FindAllMarkers function where cells in each cluster is compared to cells in all other clusters. We set the parameters such that a gene must be in 10% of all cells within that cluster, the average log fold change threshold is 0.25, and used the Wilcoxon rank sum test. Seurat's Azimuth tool was used to compare our defined cell identities to their annotated dataset[122].

Top expressed genes analysis. After assigning each cluster a cell identity, FindAllMarkers was used but in this instance instead of comparing each cluster to all other clusters, we subset one cell identity at a time and compared it against each treatment time point. Significantly expressed genes with an average log fold change >= 1.5 were identified to determine clusters with the most dynamic gene expressions across treatment time points.

T cell subset analysis. Clusters that were identified as T cells were subset from the entire PBMCs dataset for separate analysis. Dimensionality reduction and clustering was performed similarly to the previous method with minor adjustments. The joint dataset was split back into their original samples and then integrated using Harmony from the broad institute[129]. The first 20

PCs were used as input for clustering and visualization. The resolution for clustering was set to 0.7. Canonical marker detection utilized the same method with minor adjustments such that a gene must be present in 9% of cells and average log fold change threshold is 0.10. Identification of differentially expressed genes between CD4 and CD8 T cells across treatment time points utilized the previous method with a minor change to include genes present in at least 5% of cells. These values used was determined by following published best practice guides[130].

T cell receptor analysis. The accompanying scRNA-seq TCR data was analyzed and processed using Python, Scanpy, and Scirpy[131,132]. Utilizing the standard workflow suggested by Scirpy, we identified both TCRs that had either a single alpha or beta receptor chain or both. Scirpy provides a suite of functions to identify and define clonotypes. Their methods implement a network-based approach to construct a neighbour graph like Seurat's implementation. The function will define a clonotype by comparing TCR amino acid sequences. Amino acid mismatches are handled by a distance calculation determined by the Blosum62 matrix[133]. The calculated distance determines if an amino acid mismatch is acceptable in defining if two TCR sequences are similar enough to be considered the same clonotype. Processed TCR data was transferred back into R and custom scripts were used to merge this information back into the T cell Seurat object's meta data to align clonotypes to their respective T cells and clusters. Additional processing was applied to the bulk TCR dataset outputted from MiXCR using UC Berkeley SkyDeck ImmunoMind's immunarch package for the R programming lanauage[134]. Custom scripts were used to link CDR3 amino acid sequences from bulk TCR sequencing to our single-cell TCR data, effectively providing a single-cell representation of bulk PBMC and tissue clonotypes. Custom visualization scripts were developed in order to track TCR's across treatment time points and samples. Clonotype expansion was analyzed within R utilizing built in mathematical packages.

Transcription signature analysis. We derived two signatures, memory stem like and terminal effector like by performing a weighted correlation network analysis using the weighted gene co-expression network analysis (WGCNA) package[135]. We defined the memory stem signature based on markers associated with memory T cells and stem memory T cells. Similarly, we defined the terminal effector like signature based on markers associated with terminal effector and effector T cells. We used this package on CD8+ T cells. We used custom scripts to create meta cells which condenses cells from clusters into smaller bins to use WGCNA's robust

methods. From this, we were able to identify eight modules of highly correlated genes that share coexpression patterns. To score which cells and clusters were enriched for these modules we used UCell[136]. UCell evaluates gene signatures in single-cell datasets by using the Mann-Whitney U statistic to create their UCell signature score. We provided the list of genes recovered from each module for signature scoring. This revealed two dynamic modules that we later investigated and defined as memory stem like and terminal effector like. For each cluster and treatment time point the mean of both transcriptional signature scores were calculated for visualization purposes. We reclustered our CD8+ T cells utilizing the same methods from our T cell subset analysis previously described with some modifications. First, we restricted the features used to perform PCA to include only genes from both transcription signatures, we used the first 10 PCs for clustering and visualization and used a clustering resolution of 0.5.

CyTOF analysis. We used BD Life Sciences FlowJo software to analysis and clean the raw data. We then exported the processed data into R where we used flowcore and Seurat for downstream analysis. We performed similar dimensionality reduction and clustering workflows as described earlier with minor modifications. We used the first 20 PCs for clustering and visualization and used a clustering resolution of 0.5.The output of both FlowJo and Seurat was used to validate cell type proportions that we described within our scRNA-seq data.

5 Results

5.1 Single-cell immune profiling of anti-PD-1 treatment time points in r/r cHL

In order to characterize the immune cell landscape across PD-1 inhibition, we performed scRNA-seq on six samples of PBMC from one r/r cHL patient treated with anti-PD-1 therapy. Each sample corresponds to six unique time point based on treatment status (pre-treatment, on treatment, off treatment), disease state (with HL or in remission) and presence of an iRAE (present/absent). In this patient, the first time point (T1) corresponds to relapsed HL pre-treatment with a PD-1 inhibitor. The patient achieved a rapid complete response after four cycles, but this coincided with the development of pericarditis (T2). The pericarditis resolved with a short course of steroids and the patient resumed treatment and maintained a complete response for nine cycles (T3). The patient discontinued treatment and remained in remission for seven months until they experienced a HL relapse (T4). They re-started treatment for four cycles and while there was some response, some sites remained active on PET scan. They also had recurrent pericarditis (T5). The pericarditis resolved but there was clear HL progression with

further treatment (T6) (Figure 5.1a). Single-cell TCR and BCR sequencing was also performed for each sample. In total, we sequenced gene expression data from 26,925 cells that were subjected to a stringent quality control process (see methods), resulting in 25,268 cells remaining for further downstream analysis. Unsupervised clustering analysis revealed nine immune cell populations that were visualized in two dimensions using uniform manifold approximation and projection (UMAP) embeddings (Figure 5.1b).

Cell identity for each population was designated by assessing expression of canonical markers from the literature (Figure 5.1c) and correlation with an annotated reference PBMC dataset using the reference-based mapping tool Azimuth[122] (Supplementary Figure 1). The cell types identified include, CD4+ T cells (CD3D, *IL7R*, CD40LG), CD8+ T cells (CD3D, CD8A), NK cells (*KLRD1*, *FCGR3A*), B cells (CD79A, *MS4A1*), CD14+ monocytes (CD14), CD16 monocytes (*FCGR3A*), conventional dendritic cells (cDCs; CD1C, *CLEC10A*), and plasmacytoid dendritic cells (pDCs; *LILRA4*). CD4+ was not useful as marker as it was poorly expressed potentially due to being suspectable to drop out. This is in accordance with a recent study demonstrating CD4+ mRNA expression is weakly captured in droplet based scRNA-seq compared to protein level single-cell methods such as CITE-seq[137]. To compare differences in cellular composition we examined the relative proportion of cell types across treatment time points. At T4, we observed an increase in CD8+ T cells inversing the CD4+/CD8+ ratio which held throughout the remaining treatment time points (Figure 5.1d). Similar trends of increased CD8+ and decreased CD4+ T cells at relapse and onwards were observed using mass cytometry by time of flight on the same samples (Supplementary Figure 2). Given the current literature demonstrating the role of immune cells beyond T cells in ICIs[138], we first wanted to investigate changes in expression profiles of each immune cell across treatment. We performed a pairwise comparison of treatment time points for every immune cell, creating a cell specific gene list gathered from differentially expressed genes (DEGs) that met an adjusted p value cut-off of <=0.05 (Table 4.1; Figure 5.1e). Next, we wanted to determine which genes had the largest changes in up or down regulation in each gene set. We set a value of +/-1.5 as a cut-off for the average $\log_2$ fold change to further filter each gene set, resulting in 56 genes remaining (Table 4.1; Figure 5.1e). This revealed two key findings, the first being that in totality, T cells accounted for 39% of large gene expression changes across treatment and secondly, majority of upregulated genes occurred at T5 (Figure 5.1f). Notably, of these upregulated genes, *DUSP1*, *DUSP2*, *FOS*

and *JUN*, known for MAPK signalling involvement were expressed within lymphocyte cell clusters, expression of known functional genes such as *ZFP36* within the CD4+ cluster, CD69 and *NR4A2* in NK cells and type 1 interferon signature genes *IFI27*, *IFI44L*, *IFITM1* and *IFITM3* within myeloid cell clusters.

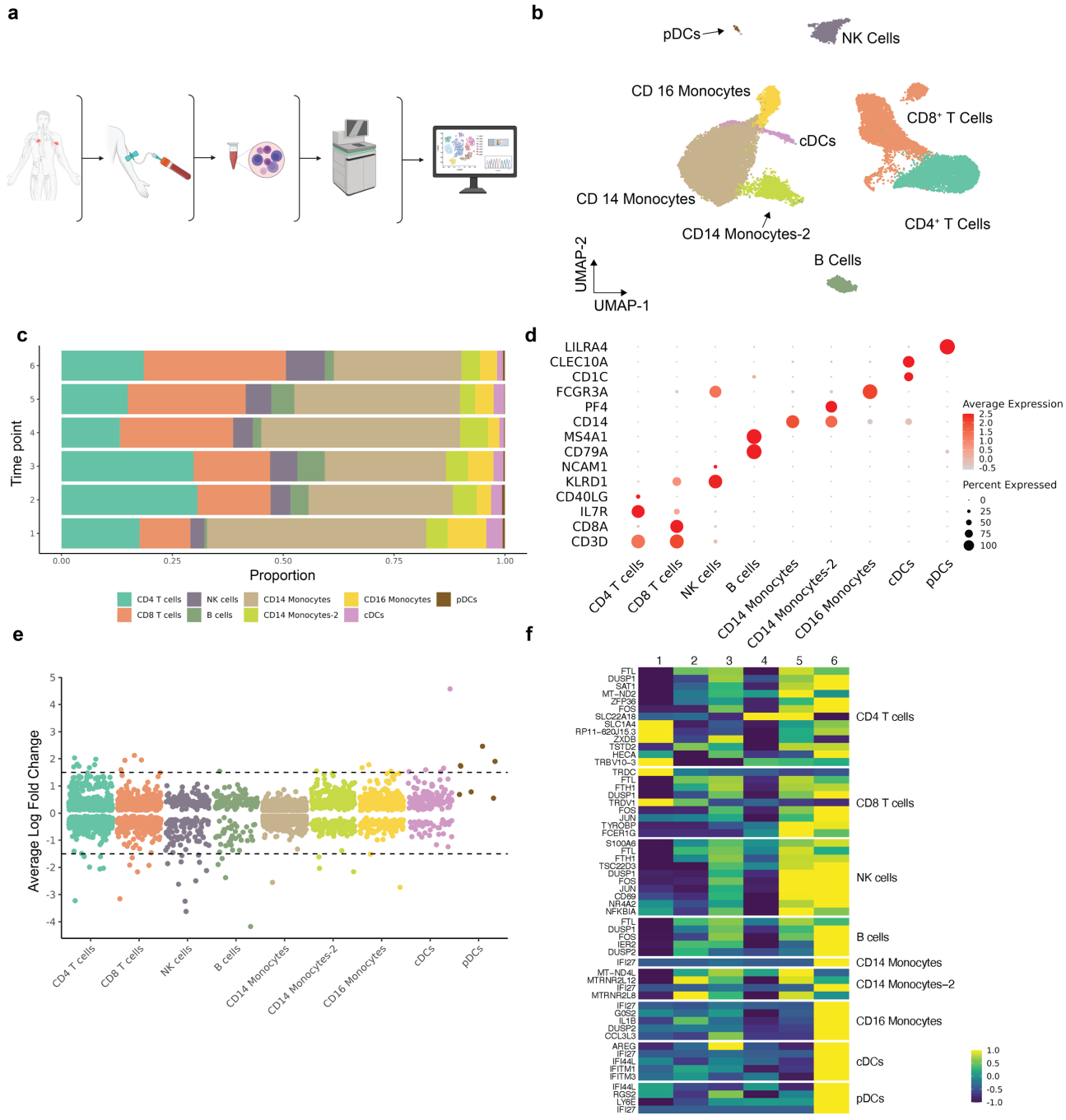

Figure 5.1. single-cell RNA sequencing results of PBMC from anti PD-1 treatment in r/r cHL. a) Schematic of dataset creation including sampling timeline to scRNA-seq. Blood samples

collected at six treatment time points: T1, relapsed cHL pre-treatment with a PD-1 inhibitor, T2, complete response after four cycles of PD-1 inhibitor but development of iRAE, T3, resolved IRAE and continuation of PD-1 inhibitor treatment, T4, discontinued treatment for seven months and disease relapsed, T5, restarted PD-1 inhibitor treatment, partial response after four cycles and reoccurrence of iRAE, T6, resolved iRAE but clear cHL progression with further PD-1 inhibitor treatment. PBMCs were isolated from blood samples, 10x libraries were prepared for each sample and sent for sequencing and data analysis. **b)** UMAP embedding of nine immune cell types from 25,268 primary immune cells of peripheral blood. Colours represent immune cell type. **c)** Proportion of each immune cell type across treatment. Y axis, treatment time point. X axis, proportion of immune cell type. **d)** Dot plot of DEGs of canonical immune cell markers. Dot sizes represent proportion of the immune cell type expressing the gene, red color scale show average expression. **e)** DEGs from comparing treatment time point per immune cell type. Each colored dot represents a DEG within an immune cell type. Dots beyond the dashed line indicate DEGs with an average log fold change greater than or equal absolute value of 1.5. **f)** Heatmap of immune cells type across each treatment time point displaying the average expression of all DEGs with an average log fold change greater than or equal absolute value of 1.5.

Table 5.1. Number of DEGs of all immune cell types across treatment.

DEGs across Timepoints	CD4+ T cells	CD8+ T cells	NK cells	B cells	CD14 monocytes	CD14 monocytes-2	CD16 monocytes	DCs	pDCs
# Of expressed genes at p value cut-off	901	855	222	146	1,955	448	415	152	7
# Of expressed genes at p value and average log_2fold change cut-off	13	9	10	5	1	4	5	5	4

5.2 Distinct T cell clusters present across all time points

Characterizing the expression profile across treatment time points of each immune cell cluster revealed that the most dynamic changes were within the T cell population. To further investigate the expression changes in T cells, we subclustered 10,593 T cells from the PBMC dataset resulting in 12 T cell subsets consisting of four CD4+ T cell clusters, seven CD8+ T cell clusters and one gammadelta T cell cluster (Figure 5.2a). Using expressed canonical markers, we further defined each T cell subset as CD4+ TH2 (*GATA3*), CD4+ TCM-1 (*SELL*, *IL7R*), CD4+

Tregs (*FOXP3*, *CTLA4*), CD4+ TH17 (*KLRB1*), CD8+ TEM-1 to CD8+ TEM-5 expressed genes associated with cytotoxicity, including (*PRF1*, *KLRG1*, *GZMB*, *GZMK*, *GZMH*), CD8+ Exhausted-1 and CD8+ Exhausted-2 expressed low but significant amounts of immune checkpoints, such as (*LAG3*, PD-1, *TIGIT*, *HAVCR2*, CTLA-4), and gammadelta T cells (TRDV3) (Figure 5.2b).

Next, we set out to profile expression changes within T cells across treatment time points. To determine which DEGs contribute the most to transcriptome differences, we collapsed all T cell subsets into two CD4+ and CD8+ T cells clusters, mitigating any large expression changes being driven from a few cells within smaller clusters. We observed distinct expression patterns in both CD4+ and CD8+ T cell clusters across treatment time points (Figure 5.2c; Figure 5.2d). CD4+ T cells at T1 expressed several genes known to be involved with active T cell function *LAT*, *KLRB1*, *CXCL13*, *ITGB1*, however the following two time points mainly had expression of mitochondrial and ribosomal genes. Interestingly, the expression of cytotoxicity-associated gene *GZMB* at T4 may suggest a cytotoxic role of CD4+ T cells. CD8+ T cells had distinct gene sets that were upregulated throughout treatment time points. Most strikingly, at T4, we observed elevated expression within a set of genes and transcription factors (*GZMB*, *PRF1*, *IL7R*, *CX3CR1*, *PRDM1*) that are functionally related to effector memory and terminally exhausted phenotypes. Interestingly, at T6, both CD4+ and CD8+ t cells had increased expression *ZFP36* and *NR4A2*, two genes that have been attributed to T cell exhaustion. Expression of *JUN* and *FOS*, genes involved in the AP-1 signaling pathway, were also expressed at this time point but mainly in CD8+ T cells. Taken together, this data suggests that the most significant phenotypical changes occur at relapse while off PD-1 inhibitor treatment. Within CD8+ T cells, we highlight *CX3CR1* and *PRDM1*, two genes involved in T cell exhaustion to have significant expression changes that have not yet been described in the context of cHL.

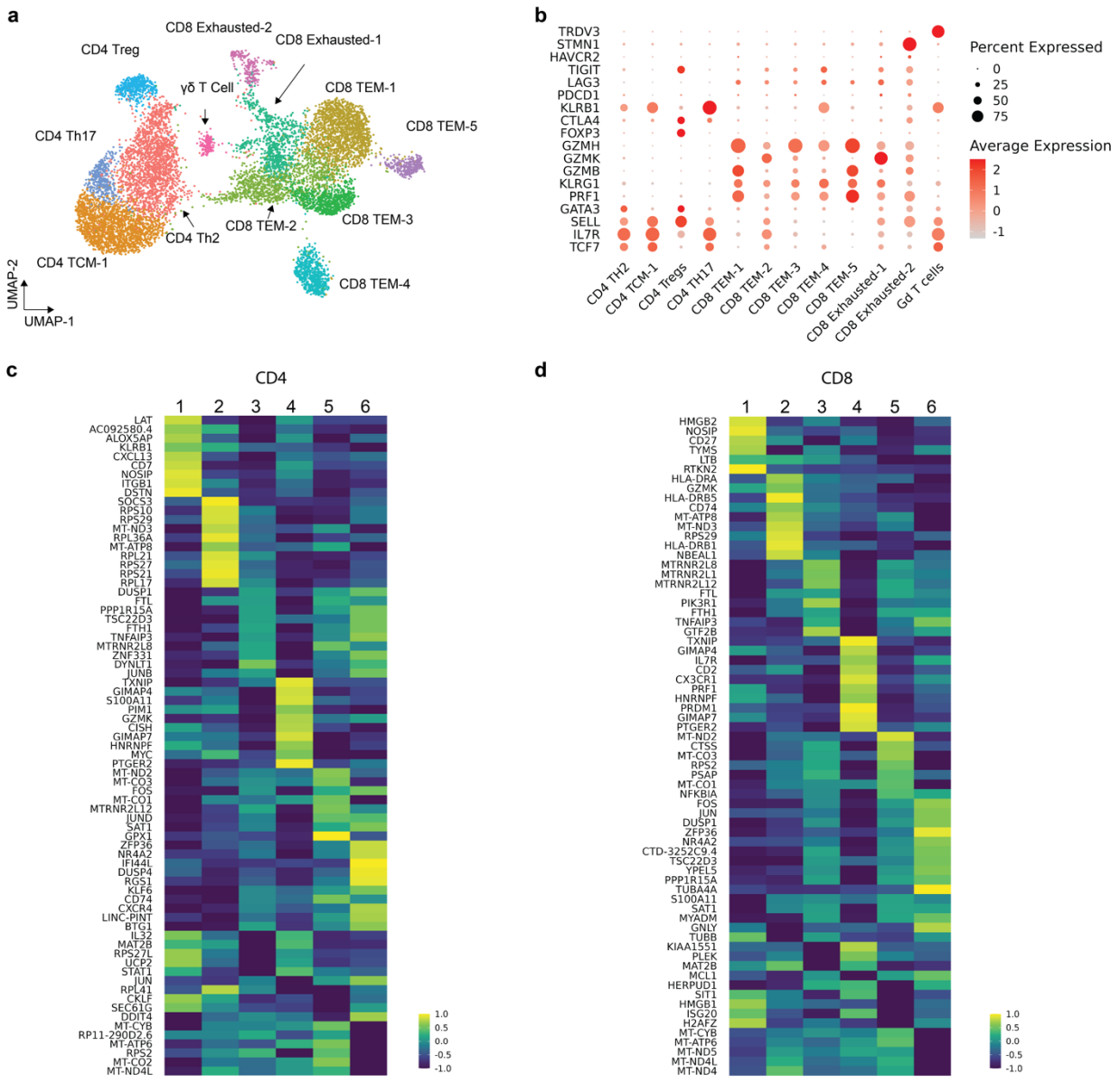

Figure 5.2. Transcriptional landscape of T cells. a) UMAP embedding of 12 T cell subsets from 10,593 T cells subset from the PBMC dataset. **b)** Dot plot of DEGs of canonical T cell subset markers. Dot sizes represent proportion of the T cell subset expressing the gene, red color scale shows average expression. **c)** Heatmap displaying the average expression of the top up and down regulated DEGs from all CD4+ T cells across each treatment time point. **d)** Heatmap displaying the average expression of the top up and down regulated DEGs from all CD8+ T cells across each treatment time point.

5.3 TCR profiling reveals clonal dynamics across PBMCs and tumor tissue

Next, we set out to further elucidate the T cell expression profile by exploring the TCR repertoire retrieved from our scRNA-seq PBMCs data along with bulk TCR sequencing. From our scRNA-seq data, we recovered TCR sequences from 39.5% of T cells, that were then assembled into clonotypes (see methods). We defined clonal expansion such that >=20 clones were considered largely expanded, $1< x < 20$ to be a small expansion and clones of one to be singletons. By projecting the clonal expansion groups onto our T cell UMAP, we observed that largely expanded clones mainly belong to CD8+ TEM-1, TEM-3, TEM-4, and TEM-5 clusters, and small clones and singletons to the rest of the CD4+ and CD8+ T cell clusters (Figure 5.3a). After resolving scRNA-seq TCR sequences into clones and their respective T cell clusters, we wanted to determine if we can track tumor tissue clones in our PBMCs data. We set out to perform bulk TCR sequencing from matched treatment time point samples of PBMCs and tumor tissue where available (see methods).

First, we used bulk PBMCs TCRs to validate our initial scRNA-seq TCR findings prior to integrating tumor tissue TCRs. We successfully matched 87% of TCRs between our scRNA-seq and bulk TCR data, with 53% of TCRs being found in tumor tissue samples (Figure 5.3b). Next, we selected the most expanded clonotypes from the bulk TCR dataset to project onto our T cell UMAP (Figure 5.3c). We observed that the top expanded clonotypes identified from both tumor tissue samples coincided with CD4+ TCM-1, CD4+ Th2, CD8+ Exhausted-1 and CD8+ TEM-2 T cell clusters. Interestingly, the two most expanded pre-PD-1 inhibitor tumor tissue clonotypes T1, were found mainly in the CD4+ Th2 cluster, with the former only occurring at the treatment naïve time point T1. Most of the top expanded bulk PBMCs TCRs overlapped the same T cell clusters that were previously shown to have large clonal expansion. This was not surprising since we expected a large overlap between bulk PBMCs and scRNA-seq PBMCs TCR data, further validating our TCR tracking method. By selecting the most expanded clonotypes from the scRNA-seq data, we were able to identify the specific TCRs that constitute the large clones observed in each T cell cluster (Figure 5.3c). TCR_3 was the only clone that had at least 100 clones in either tumor tissue samples.

To further investigate the clonal dynamics observed, we sought out to track TCRs across treatment time points (Figure 5.3d). Coinciding with the previously noted inversion of the CD4+/CD8+ ratio, tumor tissue clones that belong to CD4+ clusters diminish throughout the

treatment time points whereas CD8+ clones fluctuate but remain. Interestingly, at T4, disease relapse, we see an expansion of clone TCR_51 within the CD8+ TEM-3 cluster. Additionally, tumor tissue progressive disease clones from T6 were found in the blood within CD8+ TEM-2 and CD8+ Exhausted-1 clusters. By relating bulk TCRs to their scRNA-seq counterparts, we validated the scRNA-seq TCR data and that clones can be found in both tumor tissue and blood. We revealed that the most expanded clones found in the blood from tumor tissue or scRNA-seq PBMC data seem to be found in opposite T cell clusters. However, we did observe slight overlaps where tumour tissue clonotypes found in the blood or PBMC clonotypes occupied the same T cell cluster, suggesting tracking clonotypes may help define a dynamic phenotype state. Additionally, we show that expansion of clone TCR_51 at relapse could represent a previous clone. Although clonotypes are most likely phenotypically related which explains why they cluster together, we are still capturing T cells at a specific time point, potentially disregarding early phenotype changes. This data suggests that tracking clonotypes across treatment might help us decipher T cell heterogeneity, prompting further investigation into the transcriptional profiles of these clones. Additionally, the expansion of a clone at T4, relapse while off PD-1 inhibitor treatment supports that this time point is potentially important in elucidating the mechanism of relapse.

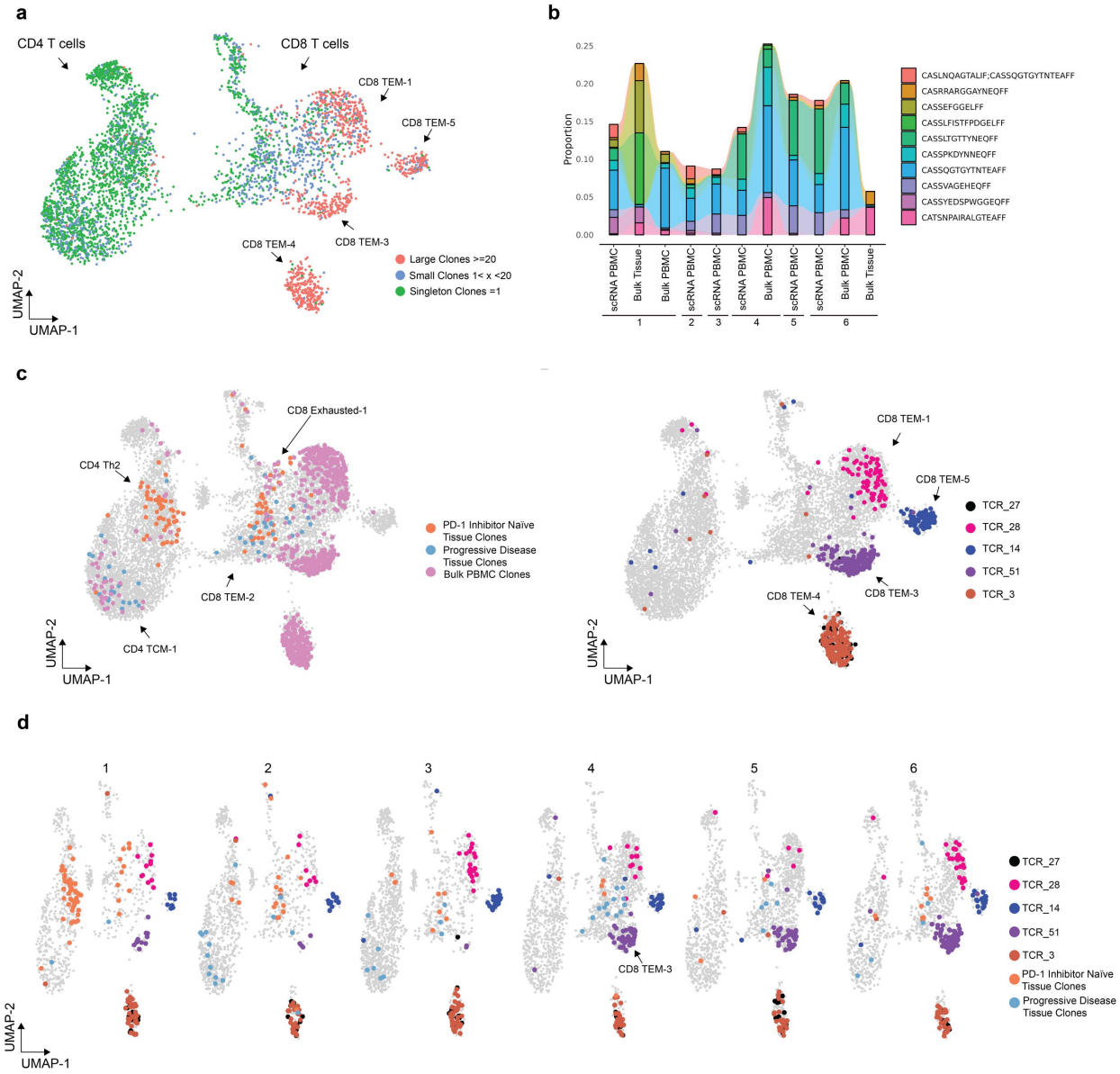

Figure 5.3 TCR repertoire analysis across tumor tissue and PBMC. a) UMAP embedding of T cells, clusters are colored by PBMC clonal expansion size. Red highlights large clones >=20, blue highlights small clones 1<x<20, and green highlights singleton clones. **b)** Proportional bar plot of the most expanded clones found from scRNA-seq PBMC and bulk PBMC and tumor tissue TCR profiling. CDR3 amino acid sequence is used to track clones. Proportion of clones Y axis, sample that contains clone X axis with additional treatment time point labeling. **c)** Left UMAP embedding of T cells where cells are colored according to most expanded clones from either scRNA-seq and bulk TCR PBMC samples or PD-1 inhibitor naïve T1 or progressive disease T6 tumor tissue. Right UMAP embedding of T cells where cells are colored according to

most expanded clones from scRNA-seq PBMC samples. **d)** UMAP embedding of T cells where cells are colored by clonotype group and tracked across each treatment time point.

5.4 Clonotype cluster preference highlights transcriptome divergence

Clonotypes within the same T cell cluster will share a similar expression profile, allowing us to utilize clonotypes as a method to trace transcriptome changes. CD4+ Th2 cluster contained the dominant treatment naïve T1 tumor tissue clonotypes of which the largest clone was only detectable within that time point. We performed a differential gene analysis of the CD4+ Th2 cluster revealing DEGs that were up/down regulated compared to the other treatment time points. By focusing on the top 30 up/down regulated DEGs, we observed an expression pattern across treatment time points of known functional T cell genes (Figure 5.4a). At T1, PD-1 inhibitor naïve, genes *ITGB1*, *LY6E*, *LAT*, and *KLRB1* were highly expressed, and their expression diminished throughout the other time points except for *LY6E* at T6, disease progression. *LY6E* and LAT are known to be expressed at T cell activation[139,140]. Interestingly, *ITGB1* has been associated with a cytotoxic and proinflammatory CD4+ subset, suggesting that this cluster may have had a cytotoxic role at this time point[141]. Genes, *TSC22D3*, *CXCR4*, *ZFP36*, and *DUSP1* are increasing in expression across the time points with their highest expression at T6, disease progression. Although this cluster has been defined as CD4+ Th2 T cells, expression of *KLRB1* is a marker for CD4+ Th17 T cells. We observed that the expression of *KLRB1* fades after T1 and expression of *TSC22D3* increases. *TSC22D3* has been known as a differentiation switch between CD4+ Th1 to Th2 phenotype and more recently as a potential regulator of Th17 cells[142,143]. This may provide insight into the heterogeneity of the CD4+ Th2 cluster across treatment.

At the relapse timepoint T4, when the patient had been not on a PD-1 inhibitor for at least 7 months, we observed an expansion of clone TCR_51 that was situated in the CD8+ TEM-3 cluster. To assess if at relapse there is a particular expression pattern present, we compared DEGs across each treatment time point (Figure 5.4b). Focusing on genes with the largest expression changes, we noted increased expression of *CX3CR1* and *PRDM1* at relapse, T4, and *NR4A2* at T6, disease progression upon PD-1 inhibitor re-treatment, which are known to be associated with a terminal exhausted phenotype. As we shown previously, besides CD4+ T cell clusters, the most expanded tumor tissue found in the blood and expanded PBMC clones could be divided into two sets of CD8+ T cell clusters. When comparing CD8+ clusters containing

expanded clones, the top DEGs revealed a gradient of expression separating both groups (Figure 5.4c). CD8+ TEM-1 and CD8+ TEM-5 expressed high levels of *GZMB*, *GNLY*, *NKG7*, *ZEB2*, *ZNF683*, and *FGFBP2* which are suggestive of a terminal effector CD8+ T cell profile. Whereas CD8+ Exhausted-1 and CD8+ TEM-2 expressed CD27, *IL7R*, *TCF7* and *SELL* which are suggestive of memory CD8+ T cell profile. CD8+ TEM-3, CD8+ TEM-4 and CD8+ Exhausted-2 T cell clusters shared variable expressions of the aforementioned genes, highlighting a transcriptomic gradient between both groups and T cell heterogeneity. Additionally, we found that *GZMK*, a cytotoxic related gene is expressed within CD8+ Exhausted-1 and CD8+ TEM-2 T cell clusters as opposed to the other clusters that have dominant expression of effector associated genes including *GZMB*. When comparing *GZMK* and *GZMB* expression, we see it also polarizes both sets of CD8+ T cell clusters (Figure 5.4d). Recently, Galletti et al have found two distinct subsets of early differentiated CD8+ memory T cells where GZMK+ cells expressed an precursor exhausted like phenotype[54]. Within our two CD8+ T cell cluster groups, expression of *GZMK* alongside memory T cell related genes may indicate T cells transitioning towards a precursor exhausted phenotype. Additionally, CD8+ TEM-3 cluster which contained the T4, relapsed expanded clonotype TCR_51 had increased expression of markers related to terminal exhaustion such as *PRDM1*, and lack of precursor exhaustion markers like *TCF7*. Taken together, this may suggest that TEM-3 is transitioning from a Tpex to a Tex phenotype as a mechanism of potential resistance to PD-1 inhibitors in cHL.

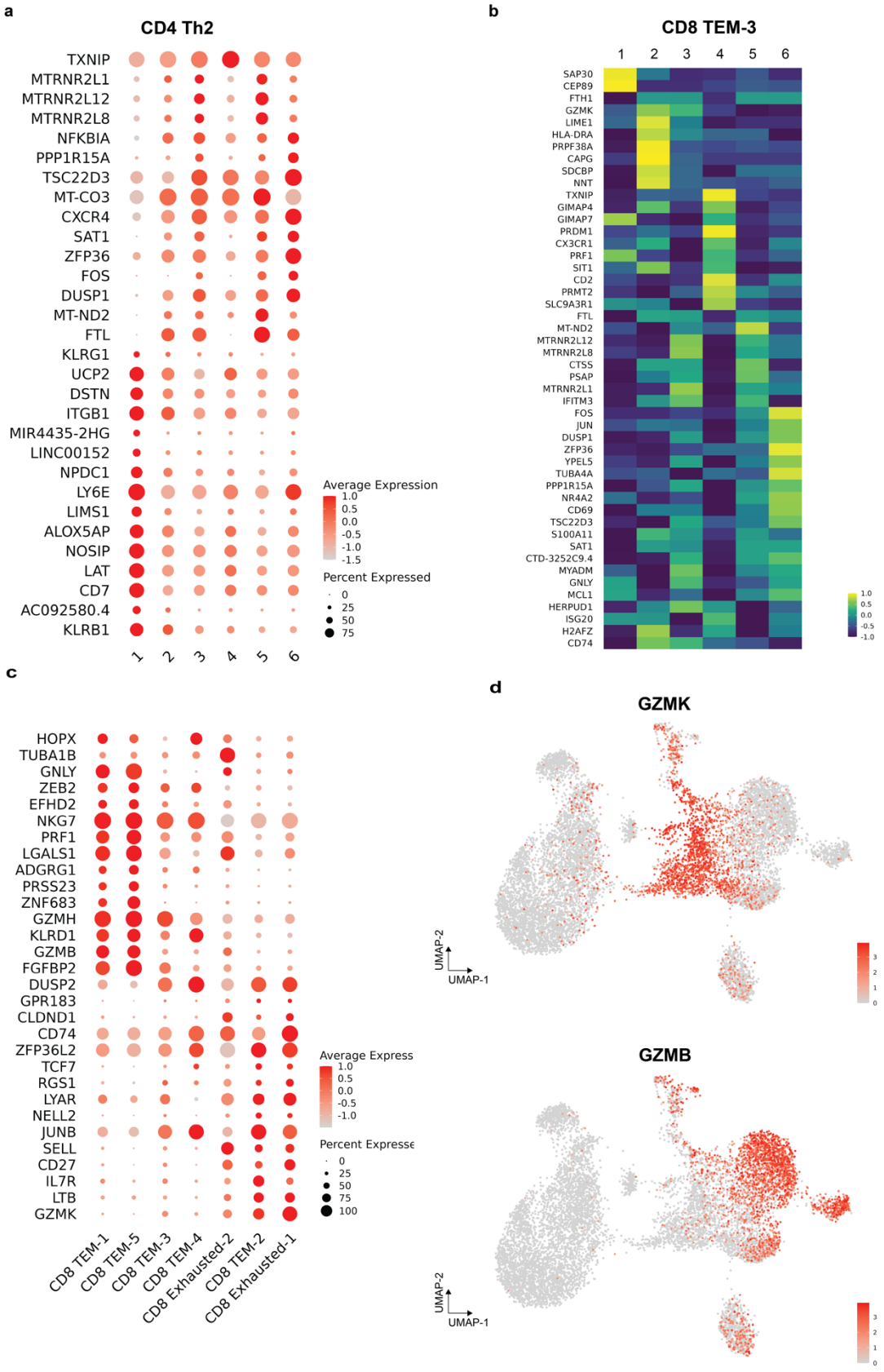
a
CD4 Th2
TXNIP
MTRNR2L1
MTRNR2L12
MTRNR2L8
NFKBIA
PPP1R15A
TSC22D3
MT-CO3
CXCR4
SAT1
ZFP36
FOS
DUSP1
MT-ND2
FTL
KLRG1
UCP2
DSTN
ITGB1
MIR4435-2HG
LINC00152
NPDC1
LY6E
LIMS1
ALOX5AP
NOSIP
LAT
CD7
AC092580.4
KLRB1
1 2 3 4 5 6
Average Expression
1.0
0.5
0.0
-0.5
-1.0
-1.5
Percent Expressed
0
25
50
75
b
CD8 TEM-3
1 2 3 4 5 6
SAP30
CEP89
FTH1
GZMK
LIME1
HLA-DRA
PRPF38A
CAPG
SDCBP
NNT
TXNIP
GIMAP4
GIMAP7
PRDM1
CX3CR1
PRF1
SIT1
CD2
PRMT2
SLC9A3R1
FTL
MT-ND2
MTRNR2L12
MTRNR2L8
CTSS
PSAP
MTRNR2L1
IFITM3
FOS
JUN
DUSP1
ZFP36
YPEL5
TUBA4A
PPP1R15A
NR4A2
CD69
TSC22D3
S100A11
SAT1
CTD-3252C9.4
MYADM
GNLY
MCL1
HERPUD1
ISG20
H2AFZ
CD74
1.0
0.5
0.0
-0.5
-1.0
c
HOPX
TUBA1B
GNLY
ZEB2
EFHD2
NKG7
PRF1
LGALS1
ADGRG1
PRSS23
ZNF683
GZMH
KLRD1
GZMB
FGFBP2
DUSP2
GPR183
CLDND1
CD74
ZFP36L2
TCF7
RGS1
LYAR
NELL2
JUNB
SELL
CD27
IL7R
LTB
GZMK
CD8 TEM-1
CD8 TEM-5
CD8 TEM-3
CD8 TEM-4
CD8 Exhausted-2
CD8 TEM-2
CD8 Exhausted-1
Average Express
1.0
0.5
0.0
-0.5
-1.0
Percent Expresse
0
25
50
75
100
d
GZMK
UMAP-2
UMAP-1
3
2
1
0
GZMB
UMAP-2
UMAP-1
3
2
1
0

Figure 5.4 Transcriptional analysis of clusters with observed clonal expansion.
a) Dot plot of top DEGs from CD4+ Th2 subset across each treatment time point. Dot sizes represent proportion of the CD4+ Th2 subset expressing the gene, red color scale show average expression. **b)** Heatmap displaying the average expression of top DEGs from CD8+ TEM-3 across each treatment time point. **c)** Dot plot of top DEGs from each CD8+ T cell subset. Dot sizes represent proportion of the CD8+ T cell subset expressing the gene, red color scale show average expression. **d)** Expression levels of *GZMK* (top) and *GZMB* (bottom) projected onto UMAP embedding. Red color scale shows gene expression level.

5.5 Identified transcriptional signatures resolve heterogenous peripheral CD8+ T cells into dynamic phenotypes

Having identified interesting DEGs when comparing CD8+ T cell clusters that contained expanded clonotypes from either tumor tissue clones found in the blood or PBMC clones, we next set out to try and further identify co-expressing genes. We applied WGCNA (see methods) to find weighted correlated networks of genes from CD8+ T cells across all time points. We identified eight modules, with two displaying the most variation of expression across the CD8+ T cell clusters (Supplementary Figure 3). When examining both modules, we found that they contain genes related to either memory, stem memory or terminal effector T cell phenotypes. One module contained 51 genes that included *TCF7*, *CXCR4*, *BTG1*, *BTG2*, markers related to memory and stem memory T cells. The other module contained 90 genes that included, *GZMB*, *FCGR3A*, *ID2*, *CX3CR1*, *FGFBP2*, *ZEB2*, *TBX21*, and *PRF1*, markers related to terminal effector and effector T cells. From this, we named the former module, memory stem like and the latter terminal effector like. We used UCell (see methods) to score both gene sets, providing expression profiles for visualization onto a CD8+ T cell UMAP. Similar to our previous finding, both memory stem like and terminal effector like signatures also demonstrate a divisive expression pattern.

Memory stem like signature includes CD8+ Exhausted-1, CD8+ TEM-2 and CD8+ TEM-4 T cell clusters (Figure 5.5a) Terminal effector like signature includes the remaining CD8+ T cell clusters besides CD8+ Exhausted-2 (Figure 5.5b). Next, we calculated the average expression of both signatures across all CD8+ T cells and then used this average as a threshold to annotate which signature does an individual CD8+ T cell most likely belong in (see methods). This effectively labels each CD8+ T cell as either signature, allowing us to determine DEGs

between both signatures. As expected, DEGs from both signatures were significantly expressed (100% of genes within memory stem like, 93% of genes within terminal effector like). The expression of the top up/down regulated DEGs across each CD8+ T cell cluster displayed a transcriptomic gradient as previously observed (Figure 5.5c). Additionally, DEGs revealed memory T cell related genes, *IL7R*, CD27, *SELL* and *LTB* were more expressed in CD8+ clusters that have higher memory stem like signature scores. Genes associated to a cytotoxic or terminal effector T cell profile, *KLRD1*, *GNLY*, *ITGB1*, *ID2*, *ZNF683* and *NKG7* were expressed in terminal effector signature enriched CD8+ T cell clusters.

Given that each CD8+ T cell cluster can be somewhat resolved into either signature, we perform supervised clustering of CD8+ T cells using features consisting of genes from both signatures (see methods). This revealed five T cell populations that were visualized through UMAP (Figure 5.5d). Interestingly, we observed that T cell subsets that share high expression of one signature clustered together compared to those with a more variable expression. Both CD8+ TEM-2 and CD8+ Exhausted-1 highly expressing memory stem like signature had clustered together, and both CD8+ TEM-1 and CD8+ TEM-5 highly expressing terminal effector like signature clustered together. Notably, CD8+ TEM-3 cluster appears to be diffused between clusters that are highly enriched in either signature. Expression of both signatures seems to be somewhat evenly expressed within the CD8+ TEM-3 subset, which may indicate that T cells within this cluster could consist of a dynamic phenotype highlighted by the polarizing apparent transcriptomic gradient. This may suggest that this cluster may be transitioning towards terminal exhaustion. Conversely, CD8+ TEM-4 subset has a high expression of memory stem like signature but does not cluster with the other two highly expressing clusters. CD8+ TEM-4 has a higher expression of terminal effector like signature compared to CD8+ TEM-2 and CD8+ Exhausted-2 which may explain why its separate and evident of another diverging dynamic phenotype. To further recapitulate this, we projected expression of both signatures and associated genes onto the reclustered UMAP. This revealed a continuum like order within the heterogenous T cell population (Figure 5.5e; Figure 5.5f).

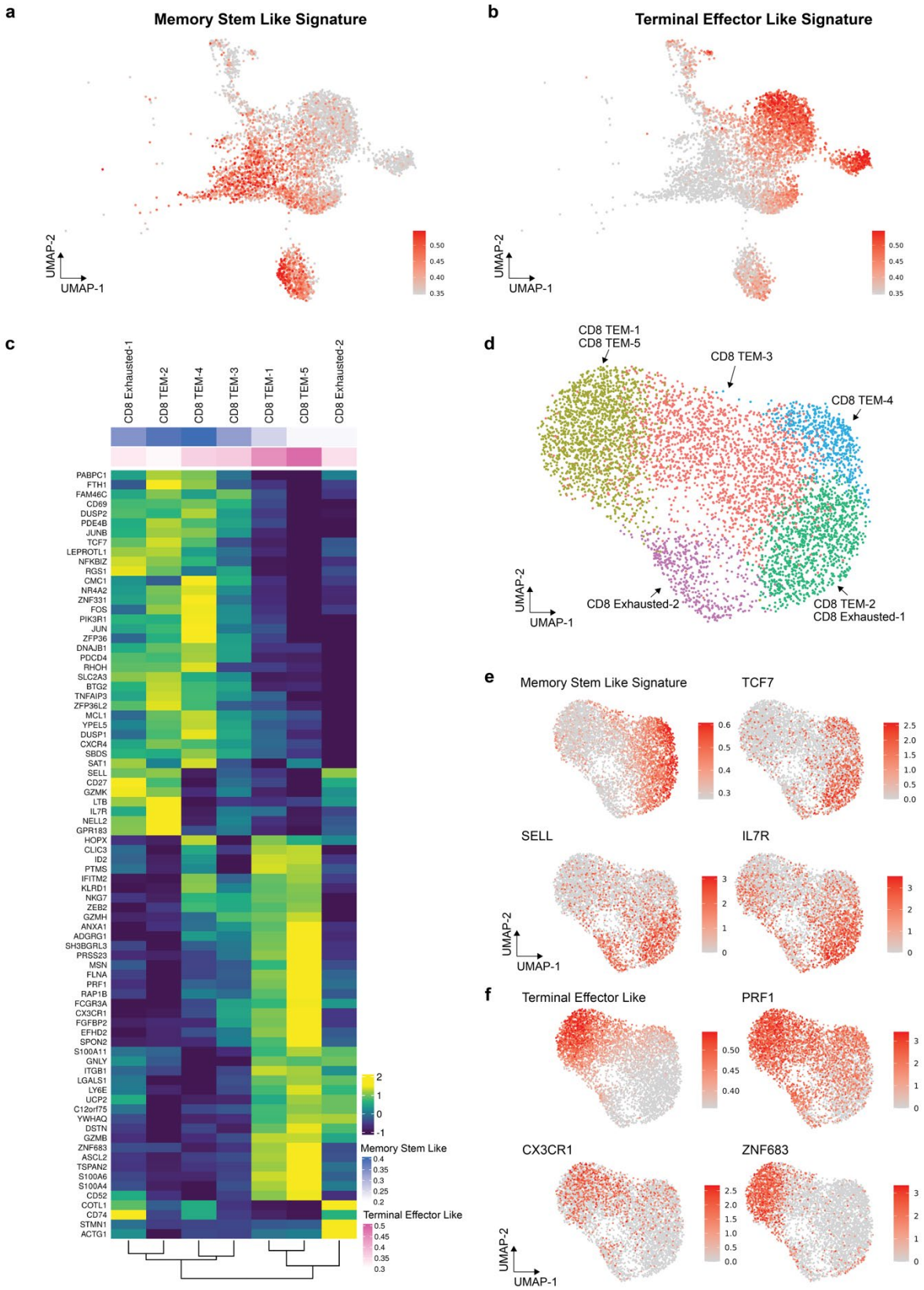
a
Memory Stem Like Signature
UMAP-2
UMAP-1
0.50
0.45
0.40
0.35
b
Terminal Effector Like Signature
UMAP-2
UMAP-1
0.50
0.45
0.40
0.35
c
CD8 Exhausted-1
CD8 TEM-2
CD8 TEM-4
CD8 TEM-3
CD8 TEM-1
CD8 TEM-5
CD8 Exhausted-2
PABPC1
FTH1
FAM46C
CD69
DUSP2
PDE4B
JUNB
TCF7
LEPROTL1
NFKBIZ
RGS1
CMC1
NR4A2
ZNF331
FOS
PIK3R1
JUN
ZFP36
DNAJB1
PDCD4
RHOH
SLC2A3
BTG2
TNFAIP3
ZFP36L2
MCL1
YPEL5
DUSP1
CXCR4
SBDS
SAT1
SELL
CD27
GZMK
LTB
IL7R
NELL2
GPR183
HOPX
CLIC3
ID2
PTMS
IFITM2
KLRD1
NKG7
ZEB2
GZMH
ANXA1
ADGRG1
SH3BGRL3
PRSS23
MSN
FLNA
PRF1
RAP1B
FCGR3A
CX3CR1
FGFBP2
EFHD2
SPON2
S100A11
GNLY
ITGB1
LGALS1
LY6E
UCP2
C12orf75
YWHAQ
DSTN
GZMB
ZNF683
ASCL2
TSPAN2
S100A6
S100A4
CD52
COTL1
CD74
STMN1
ACTG1
2
1
0
-1
Memory Stem Like
0.4
0.35
0.3
0.25
0.2
Terminal Effector Like
0.5
0.45
0.4
0.35
0.3
d
CD8 TEM-1
CD8 TEM-5
CD8 TEM-3
CD8 TEM-4
UMAP-2
UMAP-1
CD8 Exhausted-2
CD8 TEM-2
CD8 Exhausted-1
e
Memory Stem Like Signature
0.6
0.5
0.4
0.3
TCF7
2.5
2.0
1.5
1.0
0.5
0.0
SELL
3
2
1
0
IL7R
3
2
1
0
UMAP-2
UMAP-1
f
Terminal Effector Like
0.50
0.45
0.40
PRF1
3
2
1
0
CX3CR1
2.5
2.0
1.5
1.0
0.5
0.0
ZNF683
3
2
1
0
UMAP-2
UMAP-1

Figure 5.5. Identification of distinctive memory stem like and terminal effector like transcriptional signatures within heterogenous CD8+ T cells.

a) Expression levels of memory stem like signature projected onto a UMAP embedding of CD8+ T cells. Red color scale shows gene expression level. **b)** Expression levels of terminal effector like signature projected onto a UMAP embedding of CD8+ T cells. Red color scale shows gene expression level. **c)** Heatmap displaying DEGs identified by comparing cells enriched in memory stem like vs cells enriched in terminal effector like signatures. Average expression of DEGs is shown per CD8+ T cell subset. Memory stem like (blue gradient) and terminal effector like average (pink gradient) signature scores are displayed below CD8+ T cell subset names. **d)** UMAP embedding of CD8+ T cells after supervised clustering using both signature gene lists. Previous UMAP embedding labeling is applied to indicate multiple CD8+ T cell subsets have clustered together. **e)** Expression levels of memory stem like signature along with indicated genes related to memory stem phenotype projected onto a UMAP embedding of reclustered CD8+ T cells. Red color scale shows gene expression level. **f)** Expression levels of terminal effector like signature along with indicated genes related to terminal effector phenotype projected onto a UMAP embedding of reclustered CD8+ T cells. Red color scale shows gene expression level.

5.6 CX3CR1 along with precursor and terminal exhaustion markers highlight a fluctuating expression profile of T cell dysfunction.

We observed markers related to T cell exhaustion within DEGs from CD8+ T cell subsets and within both memory stem like and terminal effector like signatures. To further examine T cell exhaustion, we obtained canonical precursor and terminal exhausted T cell markers from literature and compared their expression across CD8+ T cell subsets (Figure 5.6a)[44,50,144]. CD8+ TEM-1 and CD8+ TEM-5, T cell subsets that express higher scores of terminal effector like signature shared the greatest expression of inhibitory receptors CD244, and transcription factors *ID2*, *PRDM1* that are associated to a terminally exhausted phenotype. Interestingly, CD8+ TEM-4, CD8 Exhausted-1, CD8+ TEM-2 which expressed higher scores of the memory stem like signature had a more variable expression profile that include markers from both precursor and terminal exhausted phenotypes. Precursor exhausted markers, *IL7R*, *SELL*, *TCF7* expression was mainly contained to CD8+ Exhausted-1 and CD8+ TEM-2 which agrees with their memory stem like signature score. CD8+ TEM-4 and CD8+ Exhausted-2 had strong expression of multiple

exhaustion markers. Notable high expression of *CD160*, *TOX*, *TIGIT*, *CD244*, *EOMES* and lack of *PDCD1* expression may reveal CD8+ TEM-4 to be in a transient exhausted state. Expression of *GZMB* and *GZMK* also play a role in further defining precursor and terminal exhausted phenotypes. We previously observed expression of *GZMB* and *GZMK* to be mostly concentrated to terminal effector like and memory stem like signatures respectively. Recently, groups have discovered precursor exhausted subsets expressing *GZMK*, *PDCD1*, and *TIGIT*, whereas terminally exhausted subsets expressed *GZMB*, *ZEB2*, *GNLY*, and *NGK7* which are highly expressed in our terminal effector signature[50,54]. We next sought to examine if precursor and terminal exhausted T cell marker expression varied across treatment time points of all CD8+ T cells (Figure 5.6b). This revealed a striking difference between T3, remission, and T4 relapse post treatment. At T4, terminally exhausted markers *PRDM1*, *HAVCR2*, and *ID2* were highly expressed compared to all other time points along with *CX3CR1*. Recent studies related CX3CR1+ exhausted T cells to be an transitory cell or immediate progeny of precursor exhausted T cells, with great cytotoxic and proliferation potential but risk of developing into an extremely dysfunctional exhausted terminal T cell[52,53,145].

Next, we visualized expression of *CX3CR1* along with terminal effector/exhausted markers, *TBX21*, *PRDM1*, *BATF* and *ZEB2* and precursor associated marker *TIGIT* at T3 and T4. We observed an increase in all markers and a similar pattern previously noted showing terminal exhausted related markers grouping together (Figure 5.6c). Our results are suggestive that the terminal effector like and memory like signature associated clusters may identify PBMC T cells that are between transitory states of T cell exhaustion. Taken together, the transitory states of T cell exhaustion we observed across treatment time points may suggest that PD-1 inhibitors alone cannot correct terminal exhaustion.

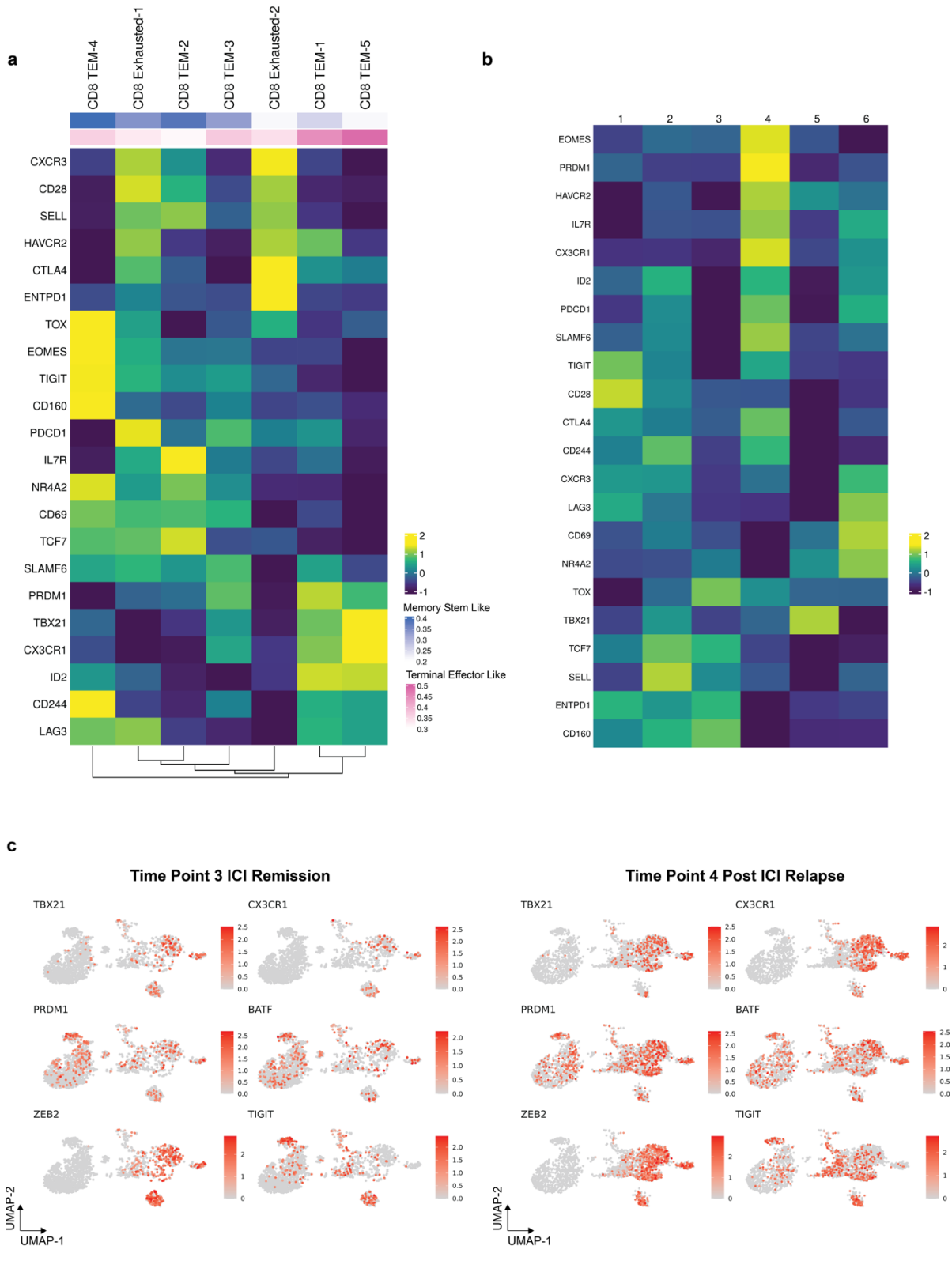
a
CD8 TEM-4
CD8 Exhausted-1
CD8 TEM-2
CD8 TEM-3
CD8 Exhausted-2
CD8 TEM-1
CD8 TEM-5
CXCR3
CD28
SELL
HAVCR2
CTLA4
ENTPD1
TOX
EOMES
TIGIT
CD160
PDCD1
IL7R
NR4A2
CD69
TCF7
SLAMF6
PRDM1
TBX21
CX3CR1
ID2
CD244
LAG3
Memory Stem Like
Terminal Effector Like
b
1
2
3
4
5
6
EOMES
PRDM1
HAVCR2
IL7R
CX3CR1
ID2
PDCD1
SLAMF6
TIGIT
CD28
CTLA4
CD244
CXCR3
LAG3
CD69
NR4A2
TOX
TBX21
TCF7
SELL
ENTPD1
CD160
c
Time Point 3 ICI Remission
Time Point 4 Post ICI Relapse
TBX21
CX3CR1
PRDM1
BATF
ZEB2
TIGIT
UMAP-2
UMAP-1

Figure 5.6. Phenotypic characterize of CD8+ T cells from transcriptional profiling of precursor and terminally exhausted T cell markers. a) Heatmap displaying average expression per cluster of precursor and terminally exhausted T cell markers. Memory stem like (blue gradient) and terminal effector like average (pink gradient) signature scores are displayed below CD8+ T cell subset names. **b)** Heatmap displaying average expression per treatment time point of precursor and terminally exhausted T cell markers. **c)** Expression levels of indicated genes related to precursor and terminally exhausted phenotype projected onto a UMAP embedding of T cells from treatment time T3 and T4. Left UMAP contains T cells from T3, ICI remission. Right UMAP contains T cells from T4 post ICI relapse. Red color scale shows gene expression level.

5.7 Immune related adverse events

Immune-related adverse events are serious side effects that can occur during ICI treatment. Within our dataset, we have two time points T2 and T5 that coincide with iRAE onset, which prompted us to identify DEGs related to either occurrence. We performed differential gene expression analysis using our entire PBMC dataset, comparing treatment time point combinations such as, T2 vs all treatment time points but excluding T5, T5 vs all treatment time points but excluding T2, and T2 and T5 together vs remaining treatment time points. Unfortunately, this analysis did not present any clear results that could provide further exploratory direction.

6 Discussion

cHL is curable in most patients with frontline chemotherapy, however, relapse remains an important clinical issue. The genetic predisposition of HRS cells to upregulate PD-L1 naturally makes cHL a prime candidate for immunotherapies targeting the PD-1 pathway. Despite the outstanding efficacy of PD-1 inhibitors in cHL, mechanisms of response are not well understood. To our knowledge, previous efforts have not utilized high-resolution transcriptomic expression profiling to study PD-1 inhibitor response in cHL patients. Using single-cell transcriptomics, we profiled peripheral immune cells of a patient with r/r cHL that initially responded but subsequently relapsed with no further response to PD-1 inhibition. Additionally, we examined T cell clonal dynamics using TCR data captured from our scRNA-seq dataset coupled with bulk TCR sequencing from time point matched PBMCs and tumor tissue. As expected, T cells displayed the most dynamic expression and cell population changes across treatment time points.

Our results reveal a decrease in CD4+ T cells occurring at relapse, expansion and retraction of T cell clones across treatment. Importantly, we identified two novel transcriptomic signatures which include markers assigned to stem memory, terminal effector, and exhaustion T cell subsets. Interestingly, we identified that at the time of relapse post PD-1 inhibition, there was increase expression of terminal effector marker *PRDM1*(encodes BLIMP-1) and *CX3CR1* in a subset of CD8+ T cells, supporting the notion that resistance to PD-1 inhibitors in this patient was associated with features of terminal exhaustion. This has never been described in HL and if confirmed in expanded cohorts, could have implications for immunotherapies of future HL patients.

The CD4+/CD8+ T cell ratio may reflect treatment response of PD-1 inhibitors. We found at PD-1 inhibitor treatment T1, T2 and T3, which relate to pre-treatment and response time points to have more CD4+ T cells than CD8+ T cells. At relapse and progressive disease timepoints T4, T5 and T6 we noted a large decrease in CD4+ T cells, inversing the ratio of CD4+/CD8+ T cells. Intriguingly, we observed that the most expanded tumor tissue clones detected within our PBMC scRNA-seq data, were mostly present in the PD-1 inhibitor-naïve time point, T1, and mainly belonged to CD4+ T cell clusters. Previous studies have described decreased circulating CD4+ T cells in patients with initial or advanced disease, which is thought to be due to the accumulation of CD4+ T cells within the TME[146,147]. Garcia-Marquetz *et al.* observed a significant increase in CD4+ T cells across treatment time points in HL patients during combinatory treatment that includes a PD-1 inhibitor[147]. Additionally, a previous longitudinal study demonstrated a reduction in circulating CD4+ $CD62L^{low}$ T cells in NSCLC patients who acquired treatment resistance after long-term response to PD-1 inhibition[148]. Recently, Cader *et al.* demonstrated that an increase in CD4+ TCR diversity within HL patients were associated to PD-1 inhibitor response and most dramatically in patients who achieved complete response[73]. We did not examine TCR diversity but with careful interpretation, this may suggest that our observation of decreased CD4+ T cells may contribute to a reduction in CD4+ TCR diversity. Given that HRS cells often have a loss of MHC Class I expression, this may highlight that CD4+ T cells have a larger role in PD-1 inhibition within HL patients. Overall, this illustrates that the proportion of CD4+ T cells may be used as a marker of treatment resistance and potentially as a mechanism for future exploration.

This study employed a novel technique to verify the presence of tumor tissue clones in the blood. By linking bulk TCR data from tumor tissue within our PBMC scRNA-seq TCR data, we were able to track clonal expansion in both blood and tumor samples. Since we could not perform scRNA-seq of the FFPE tumor tissue samples due to cells not being archived as a viable cell suspension, this technique permitted us to recover tumor tissue TCR data. This allowed us to track clones from the TME in the blood and observe their expression profile. Our data does not include scRNA-seq expression analysis of the tumor tissue therefore we cannot interpret the gene expression to be the same between clones in the blood and the TME. However, our PBMC scRNA-seq data can provide some insight into the circulating clone expression profiles.

We observed that the most expanded tumor tissue clones found in the blood were preferentially localized in similar CD8+ T cell clusters within our PMBC scRNA-seq data. In contrast, clones that were most expanded in the blood but still present in the tumor tissue all were localized in opposing CD8+ T cell clusters. By investigating the expressional differences between these opposing clusters, we identified two novel transcriptomic signatures we defined as memory stem like or terminal effector like. The memory stem like signature contained markers related to stem memory T cell and memory T cell phenotypes and terminal effector like signature contained markers related to terminally differentiated effector T cell phenotypes. There is growing evidence highlighting that exhausted T cells are heterogenous and display different functional and phenotypical profiles. Recently, researchers have also shown that Tpex cells have phenotypical similarities with stem memory T cell and memory T cell subsets whereas Tex cells have more terminal effector phenotype characteristics and more inhibitory receptors expressed[44,50,149]. Furthermore, groups have found that Tpex subtypes provide the proliferative response to PD-1 inhibitors as opposed to Tex subtypes in multiple viral and cancer studies[44,54,91,112,150]. Our results confirm that the memory and terminal effector features of Tpex and Tex cells are present within our transcriptional signatures.

By identifying DEGs between T cells that belong to either of our defined transcriptional signatures, we revealed multiple markers associated with precursor and terminal exhaustion states. T cells belonging to the memory stem like signature have high expression of *TCF7*, *IL7R*, *SELL*, *GZMK* and low expression of *PDCD1*. In contrast, T cells belonging to the terminal effector like signature have high expression of *GZMB*, *PRF1*, *ZEB2*, *ZNF683*, *PRMD1*, *TBX21* and *CX3CR1*. Several groups have linked these genes with Tpex and Tex cells. For example,

studies have shown that *GZMK* is often expressed within Tpex cells while *GZMB* is expressed within Tex[54,150,151]. The expression of *TCF7*, a defining feature of Tpex cells, upregulates *EOMES* expression which in turn upregulates *GZMK* expression[50,151]. In contrast, *PRDM1* is associated with terminal effector T cells and Tex cells as it represses *TCF7* and upregulates *GZMB* expression[50,151,152]. This is also supported by other studies which have found that *PRDM1* and *ZNF683* are expressed in terminal effector and/or resident memory T cells while also expressing *CX3CR1*, *TBX21* and *GZMB*[152,153].

The expression of *CX3CR1* and *TBX21* has also been associated with an in-between precursor and terminally exhausted state. One study found a progeny of Tpex cells expressing *CX3CR1* and *TBX21* that are not terminally exhausted, suggesting the existence of a transitory exhausted T cell state [154]. We may have found a similar state within a CD8+ T cell cluster. At relapse, T4, we observed an expansion of a CD8+ clone in the blood that was not detected in large quantities within tumor tissue. This clone falls within a CD8+ T cell cluster which has increased expression of *PRDM1*, *TBX21*, and *CX3CR1* at relapsed and disease progression timepoints, T4, T5, and T6. Our data suggests that this CD8+ T cell cluster might represent a group of circulating transitory exhausted T cells that failed to respond to PD-1 inhibitor and, like Tex cells, have decreased proliferative capacity. Terminally exhausted T cells may be a mechanism of resistance to PD-1 inhibitors within cHL. What was surprising was that when comparing the expression of these markers between T3, remission to T4 relapse we observed an increase in expression of *TIGIT*, *PRDM1*, *CX3CR1* and *TBX21*. Taken together, this may suggest that PD-1 inhibitor treatment has corrected the initial mild T cell exhausted states, evident from the lack of terminal exhaustion markers at earlier time points. However, at T4, relapse, we observed a higher exhausted state through the expression of terminal exhaustion related markers. This was followed by a slight improvement at T5, PD-1 inhibitor re-challenge, and then an increase in exhaustion markers corresponding to disease progression at T6. This suggest that PD-1 inhibitor alone may not be able to correct terminal exhaustion.

The increased expression of *CX3CR1* between T3 to T4 suggests that the *CX3CR1*/*CX3CL1* pathway may be a potential mechanisms of relapse in cHL. The expression of *CX3CR1* in CD8+ T cells has been described as a transitory exhausted T cell subset, however it has not been well described in the context of HL. HRS cells have been known to express *CX3CL1*, a chemokine which is mediated by *CX3CR1* receptors. Additionally, HRS cells are

dependent on a highly inflammatory TME to ensure their growth and survival. It is conceivable that HRS cells secreting *CX3CL1* are actively recruiting circulating CX3CR1+ T cells, which may explain the upregulation of *CX3CR1* we observed at relapse. This suggests that HRS cells may contribute to a terminal exhausted T cell state and represent another potential blood-based marker that can provide insight into PD-1 inhibitors resistance. Multiple groups have identified CD8+ T cells with proliferative and self-renewing capacities that express *CX3CR1* while also expressing terminal effector markers[154–156]. Together these phenotypic characteristics define a transitory T cell subset between Tpex and Tex states[154–156]. Additionally, CX3CR1+ CD8+ T cells often have co-expression of *ZEB2*, *TBX21*, *GZMB* and intermediate to low expression of PD-1, which our results support[154,156,157]. Multiple groups have shown the role of the *CX3CL1*/*CX3CR1* axis in the pathogenesis of several inflammatory cancers including B cell malignancies[158]. In studies investigating pancreatic ductal adenocarcinoma (PDAC) using cell lines and rat models, increased expression of *CX3CL1*/*CX3CR1* correlates with poor prognosis[159,160]. These studies also find *CX3CL1* is involved in tumor growth via JAK-STAT signaling and involved in TME crosstalk via recruitment of inflammatory cells[159,160]. However, Yamauchi *et al.* recently have shown the opposite. They demonstrated that circulating CD8+ CX3CR1+ T cells correlate with response and survival in a longitudinal study of PBMCs from NSCLC treated with PD-1 inhibitors[161].

Overall, our data supports current literature that exhaustion markers other than PD-1 are expressed at relapse post PD-1 inhibitory therapy, which can have implications for therapy[162–165]. We show that *TIGIT*, *LAG3* and *HAVCR2* (encodes TIM-3) are expressed at T4, T5 or T6 relapse and post relapse time points. These exhaustion markers are new immunotherapy targets that are being investigated therapeutically[166,167]. Clinical trials for r/r HL that use CAR T therapies to target CD30 have been reported, however it is plausible that the T cells that are apheresed from patients are from the terminal exhausted phenotype which might explain their limited activity[168,169]. It has been shown that T cell exhaustion could impair CAR T treatment efficacy[170–174]. Recently, Beider *et al* showed that CAR T cell products from patients with non-responding B cell malignancies expressed high levels of *GZMB*, *CX3CR1*, *TOX* and *EOMES* which are all markers related to exhaustion[175]. Our work may provide novel markers and phenotypes of T cell exhaustion that can be explored to improve CAR T therapy response. Finally, epigenetic mechanisms are possibly involved in modulating the transition between

precursor exhausted and terminal exhausted states. Adding an epigenetic modifier such as a histone deacetylase (HDAC) inhibitor may aid in blocking this transition. In clinical trials, HDAC inhibitors have been shown to be active in a subset of relapsed HL patients, hinting at the possibility it can be used in combination of PD-1 inhibitors to reverse terminal exhaustion[176–178]. By comparing both circulating tumor and PBMC clones, we revealed a divergent expression profile which allows us to characterize the immune landscape across PD-1 inhibitor treatment. Our results support our hypothesis that beyond PD-1, additional features of T cell exhaustion may prevent an effective response to PD-1 inhibitors in HL. Our data further supports that we initially see response to PD-1 inhibitors from precursor exhausted T cells. However, at relapse T cells begin to transition to a terminal exhausted state with little to no PD-1 inhibition response and this may be driven by HRS cells via *CX3CL1*/*CX3CR1* axis.

7 Future Directions

The limitations of this thesis mainly stem from performing scRNA-seq on samples from one patient. We only partially validated our data using bulk TCR sequencing and mass cytometry by time of flight to confirm findings of TCR clones and CD4+/CD8+ population changes. We plan to further validate our identified gene signatures at the protein level using flow cytometry on the same PBMC samples. After protein-based validation on this patient's samples, we plan to verify our findings within a larger cohort of HL patients who have differential responses to PD-1 inhibitor treatment. The need to characterize the expression profiles of the TME including rare HRS cells within a cohort of PD-1 inhibitor treated HL patients is instrumental in validating our findings and presented hypothesises. We also plan to develop techniques introduced in this thesis by prioritizing single-cell resolution that combine scRNA-seq with high resolution protein-based methods such as CITE-seq to circumvent dropout effects curbing mRNA and protein expression discrepancies[137]

To validate if features of terminal exhaustion are common across HL patients, we plan to utilize high-resolution spatial analysis tools such as CODEX[179]. In fact, we have already validated the following antibodies BLIMP-1 TCF1, CX3CR1, and soon CX3CL1 in which we will test on a tissue microarray (TMA) prepared with samples taken at diagnosis and at relapse of cHL patients, pre- and post-chemotherapy, and post PD-1 inhibitor therapy.

One future direction we want to explore is to validate the effect of CX3CL1 secretion from HRS cells on T cells. First, we plan to co-culture human CD8+ T cells from peripheral

blood of health donors in the presence of exogenous CX3CL1 protein and evaluate if CX3CR1 expression rises on T cells using flow cytometry. If CX3CL1 can increase CX3CR1 on healthy T cells, we will overexpress CX3CL1 in cHL cell lines and transfer supernatant to coculture normal human T cells to evaluate the expression of CX3CR1 as well as other cytokines and markers of terminal exhaustion. Both experiments will provide more insight into the increased expression of CX3CR1 observed within our CD8+ T cells at relapse.

8 Conclusion

Classical Hodgkin Lymphoma is an excellent model to study immunotherapy. Firstly, HRS cells are unique in their ability to curate a complex microenvironment which encourages growth and immune evasion. Furthermore, HRS cells are genetically programmed to overexpress PD-L1 allowing them to exploit the PD-1/PD-L1 axis and disarm infiltrating T cells. Although immune checkpoint inhibitors such as PD-1 blockade are highly effective in cHL, mechanisms of action and resistance remain undefined. It is crucial to have a better understanding of how T cell effector function is re-established from PD-1 inhibitors within cHL.

In this thesis, we address the limited resolution of previous cHL immunotherapy studies with efforts to increase and contribute to our shared understanding of PD-1 inhibitors in lymphoma. Therefore, we present a detailed analysis of scRNA-seq and TCR data characterizing the immune cell landscape across PD-1 inhibitor treatment of a HL patient. Our findings demonstrate that such an analysis is capable to identify the dynamic changes that occurred within the T cell population. We also demonstrated that applying novel approaches to match single-cell and bulk TCR data from PBMCs and tumor tissue allowed us to track and profile circulating clones, contributing to the identification of two novel transcriptional signatures that resolved T cell heterogeneity. Within these signatures, we identified multiple markers related to precursor and terminal exhaustion states which will be validated at the protein level and within a larger cohort.

Overall, profiling the immune cell landscape of a cHL patient has provided insight into the functional changes during PD-1 inhibitor treatment, prompting future experiments to explore the therapeutic and biomarker potentials of our findings.

Appendix I: References

1. Teras, L. R. *et al.* 2016 US lymphoid malignancy statistics by World Health Organization subtypes. *CA. Cancer J. Clin.* **66**, 443–459 (2016).

2. Connors, J. M. *et al.* Hodgkin lymphoma. *Nat. Rev. Dis. Prim.* **6**, (2020).

3. Küppers, R. The biology of Hodgkin's lymphoma. *Nat. Rev. Cancer* **9**, 15–27 (2009).

4. Piris, M. A., Medeiros, L. J. & Chang, K. C. Hodgkin lymphoma: a review of pathological features and recent advances in pathogenesis. *Pathology* **52**, 154–165 (2020).

5. Momotow, J., Borchmann, S., Eichenauer, D. A., Engert, A. & Sasse, S. Hodgkin Lymphoma—Review on Pathogenesis, Diagnosis, Current and Future Treatment Approaches for Adult Patients. *J. Clin. Med.* **10**, 1125 (2021).

6. Meti, N., Esfahani, K. & Johnson, N. A. The role of immune checkpoint inhibitors in classical hodgkin lymphoma. *Cancers (Basel).* **10**, (2018).

7. Borchmann, S. & Engert, A. The genetics of Hodgkin lymphoma: An overview and clinical implications. *Curr. Opin. Oncol.* **29**, 307–314 (2017).

8. Hudnall, S. D. & Kuppers, R. *Precision Molecular Pathology of Hodgkin Lymphoma*. (2018).

9. Schwering, I. *et al.* Loss of the B-lineage-specific gene expression program in Hodgkin and Reed-Sternberg cells of Hodgkin lymphoma. *Blood* **101**, 1505–1512 (2003).

10. Brune, V. *et al.* Origin and pathogenesis of nodular lymphocyte-predominant Hodgkin lymphoma as revealed by global gene expression analysis. *J. Exp. Med.* **205**, 2251–2268 (2008).

11. Swerdlow SH, Campo E, Harris NL, Jaffe ES, Pileri SA, Stein H, T. J. WHO Classification of Tumours of Haematopoietic and Lymphoid Tissues (Revised 4th edition). in 1–588 (2017). doi:10.1007/978-3-319-95309-0_3817.

12. Zeppa, P. & Cozzolino, I. *Hodgkin lymphoma*. *Monographs in Clinical Cytology* vol. 23 (2018).

13. Amin, M. *AJCC Cancer Staging Manual*. (American College of Surgeons, 2017).

14. Hutchings, M. PET-adapted treatment of Hodgkin lymphoma. *Blood* **134**, 1200–1201 (2019).

15. von Tresckow, B. *et al.* Dose-Intensification in Early Unfavorable Hodgkin's Lymphoma: Final Analysis of the German Hodgkin Study Group HD14 Trial. *J. Clin. Oncol.* **30**, 907–913 (2012).

16. Johnson, P. *et al.* Adapted Treatment Guided by Interim PET-CT Scan in Advanced Hodgkin's Lymphoma. *N. Engl. J. Med.* **374**, 2419–2429 (2016).

17. Radford, J. *et al.* Results of a Trial of PET-Directed Therapy for Early-Stage Hodgkin's Lymphoma. *N. Engl. J. Med.* **372**, 1598–1607 (2015).

18. Ansell, S. M. *et al.* First-line brentuximab vedotin plus chemotherapy to improve overall survival in patients with stage III/IV classical Hodgkin lymphoma: An updated analysis of ECHELON-1. *J. Clin. Oncol.* **40**, 7503–7503 (2022).

19. Vassilakopoulos, T. P. *et al.* Immunotherapy in hodgkin lymphoma: Present status and future strategies. *Cancers (Basel).* **11**, 1–38 (2019).

20. Isidori, A., Christofides, A. & Visani, G. Novel regimens prior to autologous stem cell transplantation for the management of adults with relapsed/refractory non-Hodgkin lymphoma and Hodgkin lymphoma: alternatives to BEAM conditioning. *Leuk. Lymphoma* **57**, 2499–2509 (2016).

21. Gisselbrecht, C. *et al.* Salvage regimens with autologous transplantation for relapsed large B-cell lymphoma in the rituximab era. *J. Clin. Oncol.* **28**, 4184–90 (2010).

22. Schmitz, N. *et al.* Aggressive conventional chemotherapy compared with high-dose chemotherapy with autologous haemopoietic stem-cell transplantation for relapsed chemosensitive Hodgkin's disease: a randomised trial. *Lancet* **359**, 2065–2071 (2002).

23. van de Donk, N. W. C. J. & Dhimolea, E. Brentuximab vedotin. *MAbs* **4**, 458–465 (2012).

24. Younes, A. *et al.* Results of a Pivotal Phase II Study of Brentuximab Vedotin for Patients With Relapsed or Refractory Hodgkin's Lymphoma. *J. Clin. Oncol.* **30**, 2183–2189 (2012).

25. Connors, J. M. *et al.* Brentuximab Vedotin with Chemotherapy for Stage III or IV Hodgkin's Lymphoma. *N. Engl. J. Med.* **378**, 331–344 (2018).

26. Moskowitz, C. H. *et al.* Brentuximab vedotin as consolidation therapy after autologous stem-cell transplantation in patients with Hodgkin's lymphoma at risk of relapse or progression (AETHERA): a randomised, double-blind, placebo-controlled, phase 3 trial. *Lancet* **385**, 1853–1862 (2015).

27. Rotte, A., Jin, J. Y. & Lemaire, V. Mechanistic overview of immune checkpoints to support the rational design of their combinations in cancer immunotherapy. *Ann. Oncol.* **29**, 71–83 (2018).

28. Armand, P. *et al.* Nivolumab for Relapsed/Refractory Classic Hodgkin Lymphoma After Failure of Autologous Hematopoietic Cell Transplantation: Extended Follow-Up of the Multicohort Single-Arm Phase II CheckMate 205 Trial. *J. Clin. Oncol.* **36**, 1428–1439 (2018).

29. Chen, R. *et al.* Pembrolizumab in relapsed or refractory Hodgkin lymphoma: 2-year follow-up of KEYNOTE-087. *Blood* **134**, 1144–1153 (2019).

30. Kuruvilla, J. *et al.* Pembrolizumab versus brentuximab vedotin in relapsed or refractory classical Hodgkin lymphoma (KEYNOTE-204): an interim analysis of a multicentre, randomised, open-label, phase 3 study. *Lancet. Oncol.* **22**, 512–524 (2021).

31. Das, S. & Johnson, D. B. Immune-related adverse events and anti-tumor efficacy of immune checkpoint inhibitors. *J. Immunother. Cancer* **7**, 1–11 (2019).

32. MEDZHITOV, R. & JANEWAY, C. A. Innate Immune Induction of the Adaptive Immune Response. *Cold Spring Harb. Symp. Quant. Biol.* **64**, 429–436 (1999).

33. Marshall, J. S., Warrington, R., Watson, W. & Kim, H. L. An introduction to immunology and immunopathology. *Allergy, Asthma Clin. Immunol.* **14**, 49 (2018).

34. Chaplin, D. D. Overview of the immune response. *J. Allergy Clin. Immunol.* **125**, S3–S23 (2010).

35. Cooper, M. A., Fehniger, T. A. & Caligiuri, M. A. The biology of human natural killer-cell subsets. *Trends Immunol.* **22**, 633–640 (2001).

36. Vesely, M. D., Kershaw, M. H., Schreiber, R. D. & Smyth, M. J. Natural Innate and Adaptive Immunity to Cancer. *Annu. Rev. Immunol.* **29**, 235–271 (2011).

37. Vivier, E. *et al.* Innate Lymphoid Cells: 10 Years On. *Cell* **174**, 1054–1066 (2018).

38. Yuseff, M. I., Pierobon, P., Reversat, A. & Lennon-Duménil, A. M. How B cells capture, process and present antigens: A crucial role for cell polarity. *Nat. Rev. Immunol.* **13**, 475–486 (2013).

39. Nicholson, L. B. The immune system. *Essays Biochem.* **60**, 275–301 (2016).

40. Abbas, Abul, Lichtman, Andrew, Pillai, S. Cellular and Molecular Immunology. in (Elsevier).

41. Golubovskaya, V. & Wu, L. Different Subsets of T Cells, Memory, Effector Functions, and CAR-T Immunotherapy. *Cancers (Basel).* **8**, (2016).

42. Piccirillo, C. A. Transcriptional and translational control of Foxp3+ regulatory T cell functional adaptation to inflammation. *Curr. Opin. Immunol.* **67**, 27–35 (2020).

43. Waldman, A. D., Fritz, J. M. & Lenardo, M. J. A guide to cancer immunotherapy: from T cell basic science to clinical practice. *Nat. Rev. Immunol.* **20**, 651–668 (2020).

44. Gonzalez, N. M., Zou, D., Gu, A. & Chen, W. Schrödinger's T Cells: Molecular Insights Into Stemness and Exhaustion. *Front. Immunol.* **12**, 1–12 (2021).

45. Martin, M. D. & Badovinac, V. P. Defining memory CD8 T cell. *Front. Immunol.* **9**, 1–10

(2018).

46. Gattinoni, L., Speiser, D. E., Lichterfeld, M. & Bonini, C. T memory stem cells in health and disease. *Nat. Med.* **23**, 18–27 (2017).

47. Mahnke, Y. D., Brodie, T. M., Sallusto, F., Roederer, M. & Lugli, E. The who's who of T-cell differentiation: Human memory T-cell subsets. *Eur. J. Immunol.* **43**, 2797–2809 (2013).

48. Voss, K., Luthers, C. R., Pohida, K. & Snow, A. L. Fatty Acid Synthase Contributes to Restimulation-Induced Cell Death of Human CD4 T Cells. *Front. Mol. Biosci.* **6**, (2019).

49. Wherry, E. J. & Kurachi, M. Molecular and cellular insights into T cell exhaustion. *Nat. Rev. Immunol.* **15**, 486–499 (2015).

50. Kallies, A., Zehn, D. & Utzschneider, D. T. Precursor exhausted T cells: key to successful immunotherapy? *Nat. Rev. Immunol.* **20**, 128–136 (2020).

51. Im, S. J. & Ha, S. J. Re-defining t-cell exhaustion: Subset, function, and regulation. *Immune Netw.* **20**, 1–19 (2020).

52. Utzschneider, D. T. *et al.* Early precursor T cells establish and propagate T cell exhaustion in chronic infection. *Nat. Immunol.* **21**, 1256–1266 (2020).

53. Zehn, D., Thimme, R., Lugli, E., de Almeida, G. P. & Oxenius, A. 'Stem-like' precursors are the fount to sustain persistent CD8+ T cell responses. *Nat. Immunol.* (2022) doi:10.1038/s41590-022-01219-w.

54. Galletti, G. *et al.* Two subsets of stem-like CD8+ memory T cell progenitors with distinct fate commitments in humans. *Nat. Immunol.* **21**, 1552–1562 (2020).

55. Liu, B. *et al.* Temporal single-cell tracing reveals clonal revival and expansion of precursor exhausted T cells during anti-PD-1 therapy in lung cancer. *Nat. Cancer* **3**, 108–121 (2022).

56. Mathas, S. *et al.* Elevated NF-κB p50 complex formation and Bcl-3 expression in classical Hodgkin, anaplastic large-cell, and other peripheral T-cell lymphomas. *Blood* **106**, 4287–4293 (2005).

57. Steidl, C. *et al.* Genome-wide copy number analysis of Hodgkin Reed-Sternberg cells identifies recurrent imbalances with correlations to treatment outcome. *Blood* **116**, 418–427 (2010).

58. Mottok, A. & Steidl, C. Biology of classical Hodgkin lymphoma: Implications for prognosis and novel therapies. *Blood* **131**, 1654–1665 (2018).

59. Lake, A. *et al.* Mutations of NFKBIA, encoding IκBα, are a recurrent finding in classical Hodgkin lymphoma but are not a unifying feature of non-EBV-associated cases. *Int. J.*

Cancer **125**, 1334–1342 (2009).

60. Weniger, M. A. & Küppers, R. NF-κB deregulation in Hodgkin lymphoma. *Semin. Cancer Biol.* **39**, 32–39 (2016).

61. Tiacci, E. *et al.* Pervasive mutations of JAK-STAT pathway genes in classical Hodgkin lymphoma. *Blood* **131**, 2454–2465 (2018).

62. Gunawardana, J. *et al.* Recurrent somatic mutations of PTPN1 in primary mediastinal B cell lymphoma and Hodgkin lymphoma. *Nat. Genet.* **46**, 329–335 (2014).

63. Weniger, M. A. *et al.* Mutations of the tumor suppressor gene SOCS-1 in classical Hodgkin lymphoma are frequent and associated with nuclear phospho-STAT5 accumulation. *Oncogene* **25**, 2679–2684 (2006).

64. Skinnider, B. F. & Mak, T. W. The role of cytokines in classical Hodgkin lymphoma. *Blood* **99**, 4283–4297 (2002).

65. Steidl, C., Connors, J. M. & Gascoyne, R. D. Molecular pathogenesis of hodgkin's lymphoma: Increasing evidence of the importance of the microenvironment. *J. Clin. Oncol.* **29**, 1812–1826 (2011).

66. Visser, L., Veldman, J., Poppema, S., van den Berg, A. & Diepstra, A. Microenvironment, cross-talk, and immune escape mechanisms. *Hematol. Malig.* 69–86 (2020) doi:10.1007/978-3-030-32482-7_4.

67. Schreck, S. *et al.* Prognostic impact of tumour-infiltrating Th2 and regulatory T cells in classical Hodgkin lymphoma. *Hematol. Oncol.* **27**, 31–39 (2009).

68. Atayar, Ç. *et al.* Hodgkin's lymphoma associated T-cells exhibit a transcription factor profile consistent with distinct lymphoid compartments. *J. Clin. Pathol.* **60**, 1092–1097 (2007).

69. Cader, F. Z. *et al.* Mass cytometry of Hodgkin lymphoma reveals a CD41 regulatory T-cell–rich and exhausted T-effector microenvironment. *Blood* **132**, 825–836 (2018).

70. Greaves, P. *et al.* Defining characteristics of classical Hodgkin lymphoma. *Blood* **122**, 2856–2863 (2013).

71. Aoki, T. *et al.* Single-cell transcriptome analysis reveals disease-defining t-cell subsets in the tumor microenvironment of classic hodgkin lymphoma. *Cancer Discov.* **10**, 406–421 (2020).

72. Ferrarini, I., Rigo, A., Visco, C., Krampera, M. & Vinante, F. The evolving knowledge on t and nk cells in classic hodgkin lymphoma: Insights into novel subsets populating the immune microenvironment. *Cancers (Basel).* **12**, 1–20 (2020).

73. Cader, F. Z. *et al.* A peripheral immune signature of responsiveness to PD-1 blockade in

patients with classical Hodgkin lymphoma. *Nat. Med.* **26**, 1468–1479 (2020).

74. Takata, K. *et al.* Identification of LAG3+ T Cell Populations in the Tumor Microenvironment of Classical Hodgkin Lymphoma and B-Cell Non-Hodgkin Lymphoma. *Blood* **136**, 19–19 (2020).

75. Liu, W. R. & Shipp, M. A. Signaling pathways and immune evasion mechanisms in classical Hodgkin lymphoma. *Blood* **130**, 2265–2270 (2017).

76. Reichel, J. *et al.* Flow sorting and exome sequencing reveal the oncogenome of primary Hodgkin and Reed-Sternberg cells. *Blood* **125**, 1061–1072 (2015).

77. Roemer, M. G. M. *et al.* Classical Hodgkin lymphoma with reduced β2M/MHC class i expression is associated with inferior outcome independent of 9p24.1 status. *Cancer Immunol. Res.* **4**, 910–916 (2016).

78. Steidl, C. *et al.* MHC class II transactivator CIITA is a recurrent gene fusion partner in lymphoid cancers. *Nature* **471**, 377–383 (2011).

79. Diepstra, A. *et al.* HLA class II expression by Hodgkin Reed-Sternberg cells is an independent prognostic factor in classical Hodgkin's lymphoma. *J. Clin. Oncol.* **25**, 3101–3108 (2007).

80. Wein, F. *et al.* Complex immune evasion strategies in classical Hodgkin lymphoma. *Cancer Immunol. Res.* **5**, 1122–1132 (2017).

81. Murray, P. J. & Wynn, T. A. Protective and pathogenic functions of macrophage subsets. *Nat. Rev. Immunol.* **11**, 723–737 (2011).

82. Tudor, C. S. *et al.* Macrophages and dendritic cells as actors in the immune reaction of classical hodgkin lymphoma. *PLoS One* **9**, 1–24 (2014).

83. Barros, M. H. M., Segges, P., Vera-Lozada, G., Hassan, R. & Niedobitek, G. Macrophage polarization reflects T cell composition of tumor microenvironment in pediatric classical Hodgkin lymphoma and has impact on survival. *PLoS One* **10**, 1–19 (2015).

84. Ruella, M. *et al.* Overcoming the immunosuppressive tumor microenvironment of Hodgkin lymphoma using chimeric antigen receptor T cells. *Cancer Discov.* **7**, 1154–1167 (2017).

85. De Re, Caggiari, Repetto, Mussolin & Mascarin. Classical Hodgkin's Lymphoma in the Era of Immune Checkpoint Inhibition. *J. Clin. Med.* **8**, 1596 (2019).

86. Green, M. R. *et al.* Integrative analysis reveals selective 9p24.1 amplification, increased PD-1 ligand expression, and further induction via JAK2 in nodular sclerosing Hodgkin lymphoma and primary mediastinal large B-cell lymphoma. *Blood* **116**, 3268–3277 (2010).

87. Green, M. R. *et al.* Constitutive AP-1 activity and EBV infection induce PD-l1 in Hodgkin lymphomas and posttransplant lymphoproliferative disorders: Implications for targeted therapy. *Clin. Cancer Res.* **18**, 1611–1618 (2012).

88. Carey, C. D. *et al.* Topological analysis reveals a PD-L1-associated microenvironmental niche for Reed-Sternberg cells in Hodgkin lymphoma. *Blood* **130**, 2420–2430 (2017).

89. Timmerman, J. *et al.* Favezelimab (anti–LAG-3) plus pembrolizumab in patients with relapsed or refractory (R/R) classical Hodgkin lymphoma (cHL) after anti–PD-1 treatment: An open-label phase 1/2 study. *J. Clin. Oncol.* **40**, 7545–7545 (2022).

90. Tobin, J. W. D., Bednarska, K., Campbell, A. & Keane, C. PD-1 and LAG-3 Checkpoint Blockade: Potential Avenues for Therapy in B-Cell Lymphoma. *Cells* **10**, (2021).

91. Im, S. J. *et al.* Defining CD8+ T cells that provide the proliferative burst after PD-1 therapy. *Nature* **537**, 417–421 (2016).

92. Kim, K. *et al.* Single-cell transcriptome analysis reveals TOX as a promoting factor for T-cell exhaustion and a predictor for anti-PD1 responses in human cancer. *bioRxiv* 1–16 (2019) doi:10.1101/641316.

93. Mann, T. H. & Kaech, S. M. Tick-TOX, it's time for T cell exhaustion. *Nat. Immunol.* **20**, 1092–1094 (2019).

94. Alfei, F. *et al.* TOX reinforces the phenotype and longevity of exhausted T cells in chronic viral infection. *Nature* **571**, 265–269 (2019).

95. El Halabi, L. *et al.* Expression of the Immune Checkpoint Regulators LAG-3 and TIM-3 in Classical Hodgkin Lymphoma. *Clin. Lymphoma, Myeloma Leuk.* **21**, 257-266.e3 (2021).

96. Li, W. *et al.* Expression of the immune checkpoint receptor TIGIT in Hodgkin's lymphoma. *BMC Cancer* **18**, 1209 (2018).

97. Hommes, J. W., Verheijden, R. J., Suijkerbuijk, K. P. M. & Hamann, D. Biomarkers of Checkpoint Inhibitor Induced Immune-Related Adverse Events—A Comprehensive Review. *Front. Oncol.* **10**, (2021).

98. Jia, X.-H. *et al.* The biomarkers related to immune related adverse events caused by immune checkpoint inhibitors. *J. Exp. Clin. Cancer Res.* **39**, 284 (2020).

99. Head, L. *et al.* Biomarkers to predict immune-related adverse events with checkpoint inhibitors. *J. Clin. Oncol.* **37**, 131–131 (2019).

100. Maçon-Lemaître, L. & Triebel, F. The negative regulatory function of the lymphocyte-activation gene-3 co-receptor (CD223) on human T cells. *Immunology* **115**, 170–178 (2005).

101. Anderson, A. C. Tim-3: An emerging target in the cancer immunotherapy landscape. *Cancer Immunol. Res.* **2**, 393–398 (2014).

102. Harjunpää, H. & Guillerey, C. TIGIT as an emerging immune checkpoint. *Clin. Exp. Immunol.* **200**, 108–119 (2020).

103. McKinnon, K. M. Flow Cytometry: An Overview. *Curr. Protoc. Immunol.* **120**, (2018).

104. Spitzer, M. H. & Nolan, G. P. Mass Cytometry: Single Cells, Many Features. *Cell* **165**, 780–791 (2016).

105. Tang, F. *et al.* mRNA-Seq whole-transcriptome analysis of a single cell. *Nat. Methods* **6**, 377–382 (2009).

106. Kolodziejczyk, A. A., Kim, J. K., Svensson, V., Marioni, J. C. & Teichmann, S. A. The Technology and Biology of Single-Cell RNA Sequencing. *Mol. Cell* **58**, 610–620 (2015).

107. Zheng, G. X. Y. *et al.* Massively parallel digital transcriptional profiling of single cells. *Nat. Commun.* **8**, 14049 (2017).

108. Singh, M. *et al.* High-throughput targeted long-read single cell sequencing reveals the clonal and transcriptional landscape of lymphocytes. *Nat. Commun.* **10**, 3120 (2019).

109. Yao, C. *et al.* Single-cell RNA-seq reveals TOX as a key regulator of CD8+ T cell persistence in chronic infection. *Nat. Immunol.* **20**, 890–901 (2019).

110. Zhang, F. *et al.* Dynamics of peripheral T cell clones during PD-1 blockade in non-small cell lung cancer. *Cancer Immunol. Immunother.* **69**, 2599–2611 (2020).

111. Liu, B. *et al. Temporal single-cell tracing reveals clonal revival and expansion of precursor exhausted T cells during anti-PD-1 therapy in lung cancer*. *Nature Cancer* vol. 3 (2022).

112. Sade-Feldman, M. *et al.* Defining T Cell States Associated with Response to Checkpoint Immunotherapy in Melanoma. *Cell* **175**, 998-1013.e20 (2018).

113. Guo, X. *et al.* Global characterization of T cells in non-small-cell lung cancer by single-cell sequencing. *Nat. Med.* **24**, 978–985 (2018).

114. Yost, K. E. *et al.* Clonal replacement of tumor-specific T cells following PD-1 blockade. *Nat. Med.* **25**, 1251–1259 (2019).

115. Li, H. *et al.* Dysfunctional CD8 T Cells Form a Proliferative, Dynamically Regulated Compartment within Human Melanoma. *Cell* **176**, 775-789.e18 (2019).

116. Zhang, J. Y. *et al.* Single-cell landscape of immunological responses in patients with COVID-19. *Nat. Immunol.* **21**, 1107–1118 (2020).

117. Corridoni, D. *et al. Single-cell atlas of colonic CD8+ T cells in ulcerative colitis*. *Nature*

Medicine vol. 26 (Springer US, 2020).

118. Pauken, K. E. *et al.* Single-cell analyses identify circulating anti-tumor CD8 T cells and markers for their enrichment. *J. Exp. Med.* **218**, (2021).

119. Lozano, A. X. *et al.* T cell characteristics associated with toxicity to immune checkpoint blockade in patients with melanoma. *Nat. Med.* (2022) doi:10.1038/s41591-021-01623-z.

120. Bolotin, D. A. *et al.* MiXCR: software for comprehensive adaptive immunity profiling. *Nat. Methods* **12**, 380–381 (2015).

121. Team, R. C. R: A langauge and Environment for Statistical Computing.

122. Hao, Y. *et al.* Integrated analysis of multimodal single-cell data. *Cell* **184**, 3573-3587.e29 (2021).

123. Young, M. D. & Behjati, S. SoupX removes ambient RNA contamination from droplet-based single-cell RNA sequencing data. *Gigascience* **9**, (2020).

124. Wolock, S. L., Lopez, R. & Klein, A. M. Scrublet: Computational Identification of Cell Doublets in Single-Cell Transcriptomic Data. *Cell Syst.* **8**, 281-291.e9 (2019).

125. McInnes, L., Healy, J., Saul, N. & Großberger, L. UMAP: Uniform Manifold Approximation and Projection. *J. Open Source Softw.* **3**, 861 (2018).

126. Xu, C. & Su, Z. Identification of cell types from single-cell transcriptomes using a novel clustering method. *Bioinformatics* **31**, 1974–1980 (2015).

127. Levine, J. H. *et al.* Data-Driven Phenotypic Dissection of AML Reveals Progenitor-like Cells that Correlate with Prognosis. *Cell* **162**, 184–97 (2015).

128. Blondel, V. D., Guillaume, J.-L., Lambiotte, R. & Lefebvre, E. Fast unfolding of communities in large networks. *J. Stat. Mech. Theory Exp.* **2008**, P10008 (2008).

129. Korsunsky, I. *et al.* Fast, sensitive and accurate integration of single-cell data with Harmony. *Nat. Methods* **16**, 1289–1296 (2019).

130. Luecken, M. D. & Theis, F. J. Current best practices in single-cell RNA-seq analysis: a tutorial. *Mol. Syst. Biol.* **15**, (2019).

131. Sturm, G. *et al.* Scirpy: a Scanpy extension for analyzing single-cell T-cell receptor-sequencing data. *Bioinformatics* **36**, 4817–4818 (2020).

132. Wolf, F. A., Angerer, P. & Theis, F. J. SCANPY: large-scale single-cell gene expression data analysis. *Genome Biol.* **19**, 15 (2018).

133. Dash, P. *et al.* Quantifiable predictive features define epitope-specific T cell receptor repertoires. *Nature* **547**, 89–93 (2017).

134. Popov, A. *et al.* immunomind/immunarch: Immunarch 0.6.9. (2022) doi:10.5281/ZENODO.6599744.

135. Langfelder, P. & Horvath, S. WGCNA: an R package for weighted correlation network analysis. *BMC Bioinformatics* **9**, 559 (2008).

136. Andreatta, M. & Carmona, S. J. UCell: Robust and scalable single-cell gene signature scoring. *Comput. Struct. Biotechnol. J.* **19**, 3796–3798 (2021).

137. Li, J., Zhang, Y., Yang, C. & Rong, R. Discrepant mRNA and Protein Expression in Immune Cells. *Curr. Genomics* **21**, 560–563 (2020).

138. Petitprez, F., Meylan, M., de Reyniès, A., Sautès-Fridman, C. & Fridman, W. H. The Tumor Microenvironment in the Response to Immune Checkpoint Blockade Therapies. *Front. Immunol.* **11**, 1–11 (2020).

139. Balagopalan, L. *et al.* Enhanced T-cell signaling in cells bearing linker for activation of T-cell (LAT) molecules resistant to ubiquitylation. *Proc. Natl. Acad. Sci.* **108**, 2885–2890 (2011).

140. Saitoh, S. *et al.* Modulation of TCR-mediated signaling pathway by thymic shared antigen-1 (TSA-1)/stem cell antigen-2 (Sca-2). *J. Immunol.* **155**, 5574–81 (1995).

141. Nicolet, B. P., Guislain, A. & Wolkers, M. C. CD29 Enriches for Cytotoxic Human CD4 + T Cells. *J. Immunol.* **207**, 2966–2975 (2021).

142. Riccardi, C. GILZ as a mediator of the anti-inflammatory effects of glucocorticoids. *Front. Endocrinol. (Lausanne).* **6**, 1–6 (2015).

143. Cannarile, L., Delfino, D. V., Adorisio, S., Riccardi, C. & Ayroldi, E. Implicating the Role of GILZ in Glucocorticoid Modulation of T-Cell Activation. *Front. Immunol.* **10**, 1823 (2019).

144. Dolina, J. S., Van Braeckel-Budimir, N., Thomas, G. D. & Salek-Ardakani, S. CD8+ T Cell Exhaustion in Cancer. *Front. Immunol.* **12**, 1–13 (2021).

145. Collier, J. L., Weiss, S. A., Pauken, K. E., Sen, D. R. & Sharpe, A. H. Not-so-opposite ends of the spectrum: CD8+ T cell dysfunction across chronic infection, cancer and autoimmunity. *Nat. Immunol.* **22**, 809–819 (2021).

146. Maggi, E. *et al.* Role of T Cells in the Pathogenesis of Hodgkin's Disease. in 141–164 (1992). doi:10.1016/B978-0-12-364933-1.50011-4.

147. Garcia-Marquez, M. A. *et al.* Reverted exhaustion phenotype of circulating lymphocytes as immune correlate of anti-PD1 first-line treatment in Hodgkin lymphoma. *Leukemia* **36**, 760–771 (2022).

148. Kagamu, H. *et al.* CD4+ T-cell Immunity in the Peripheral Blood Correlates with

Response to Anti-PD-1 Therapy. *Cancer Immunol. Res.* **8**, 334–344 (2020).

149. Dominguez, C. X. *et al.* The transcription factors ZEB2 and T-bet cooperate to program cytotoxic T cell terminal differentiation in response to LCMV viral infection. *J. Exp. Med.* **212**, 2041–2056 (2015).

150. Miller, B. C. *et al.* Subsets of exhausted CD8+ T cells differentially mediate tumor control and respond to checkpoint blockade. *Nat. Immunol.* **20**, 326–336 (2019).

151. Mogilenko, D. A. *et al.* Comprehensive Profiling of an Aging Immune System Reveals Clonal GZMK+ CD8+ T Cells as Conserved Hallmark of Inflammaging. *Immunity* **54**, 99-115.e12 (2021).

152. Kragten, N. A. M. *et al.* Blimp-1 induces and Hobit maintains the cytotoxic mediator granzyme B in CD8 T cells. *Eur. J. Immunol.* **48**, 1644–1662 (2018).

153. Oja, A. E. *et al.* The Transcription Factor Hobit Identifies Human Cytotoxic CD4+ T Cells. *Front. Immunol.* **8**, (2017).

154. Hudson, W. H. *et al.* Proliferating Transitory T Cells with an Effector-like Transcriptional Signature Emerge from PD-1+ Stem-like CD8+ T Cells during Chronic Infection. *Immunity* **51**, 1043-1058.e4 (2019).

155. Buchholz, V. R. & Busch, D. H. Back to the Future: Effector Fate during T Cell Exhaustion. *Immunity* **51**, 970–972 (2019).

156. Belk, J. A., Daniel, B. & Satpathy, A. T. Epigenetic regulation of T cell exhaustion. *Nat. Immunol.* **23**, 848–860 (2022).

157. Zander, R. *et al.* CD4+ T Cell Help Is Required for the Formation of a Cytolytic CD8+ T Cell Subset that Protects against Chronic Infection and Cancer. *Immunity* **51**, 1028-1042.e4 (2019).

158. Ferretti, E., Pistoia, V. & Corcione, A. Role of Fractalkine/CX3CL1 and Its Receptor in the Pathogenesis of Inflammatory and Malignant Diseases with Emphasis on B Cell Malignancies. *Mediators Inflamm.* **2014**, 1–10 (2014).

159. Conroy, M. J. & Lysaght, J. CX3CL1 Signaling in the Tumor Microenvironment. in 1–12 (2020). doi:10.1007/978-3-030-36667-4_1.

160. Huang, L. *et al.* Fractalkine Upregulates Inflammation through CX3CR1 and the Jak–Stat Pathway in Severe Acute Pancreatitis Rat Model. *Inflammation* **35**, 1023–1030 (2012).

161. Yamauchi, T. *et al.* T-cell CX3CR1 expression as a dynamic blood-based biomarker of response to immune checkpoint inhibitors. *Nat. Commun.* **12**, 1402 (2021).

162. Donini, C., D'Ambrosio, L., Grignani, G., Aglietta, M. & Sangiolo, D. Next generation immune-checkpoints for cancer therapy. *J. Thorac. Dis.* **10**, S1581–S1601 (2018).

163. Nowicki, T. S., Hu-Lieskovan, S. & Ribas, A. Mechanisms of Resistance to PD-1 and PD-L1 Blockade. *Cancer J.* **24**, 47–53.

164. Lei, Q., Wang, D., Sun, K., Wang, L. & Zhang, Y. Resistance Mechanisms of Anti-PD1/PDL1 Therapy in Solid Tumors. *Front. Cell Dev. Biol.* **8**, (2020).

165. Jenkins, R. W., Barbie, D. A. & Flaherty, K. T. Mechanisms of resistance to immune checkpoint inhibitors. *Br. J. Cancer* **118**, 9–16 (2018).

166. Wei, Y. & Li, Z. LAG3-PD-1 Combo Overcome the Disadvantage of Drug Resistance. *Front. Oncol.* **12**, 831407 (2022).

167. Gaynor, N., Crown, J. & Collins, D. M. Immune checkpoint inhibitors: Key trials and an emerging role in breast cancer. *Semin. Cancer Biol.* **79**, 44–57 (2022).

168. Ramos, C. A. *et al.* Anti-CD30 CAR-T Cell Therapy in Relapsed and Refractory Hodgkin Lymphoma. *J. Clin. Oncol.* **38**, 3794–3804 (2020).

169. Ramos, C. A. *et al.* CD30-Chimeric Antigen Receptor (CAR) T Cells for Therapy of Hodgkin Lymphoma (HL). *Blood* **132**, 680–680 (2018).

170. Ramos, C. A., Heslop, H. E. & Brenner, M. K. CAR-T Cell Therapy for Lymphoma. *Annu. Rev. Med.* **67**, 165–83 (2016).

171. Mardiana, S. & Gill, S. CAR T Cells for Acute Myeloid Leukemia: State of the Art and Future Directions. *Front. Oncol.* **10**, (2020).

172. Poorebrahim, M. *et al.* Counteracting CAR T cell dysfunction. *Oncogene* **40**, 421–435 (2021).

173. Gumber, D. & Wang, L. D. Improving CAR-T immunotherapy: Overcoming the challenges of T cell exhaustion. *eBioMedicine* **77**, 103941 (2022).

174. Lynn, R. C. *et al.* c-Jun overexpression in CAR T cells induces exhaustion resistance. *Nature* **576**, 293–300 (2019).

175. Beider, K. *et al.* Molecular and Functional Signatures Associated with CAR T Cell Exhaustion and Impaired Clinical Response in Patients with B Cell Malignancies. *Cells* **11**, (2022).

176. Chen, I.-C., Sethy, B. & Liou, J.-P. Recent Update of HDAC Inhibitors in Lymphoma. *Front. cell Dev. Biol.* **8**, 576391 (2020).

177. Janku, F. *et al.* Safety and Efficacy of Vorinostat Plus Sirolimus or Everolimus in Patients with Relapsed Refractory Hodgkin Lymphoma. *Clin. Cancer Res.* **26**, 5579–5587 (2020).

178. Buglio, D. & Younes, A. Histone deacetylase inhibitors in Hodgkin lymphoma. *Invest. New Drugs* **28 Suppl 1**, S21-7 (2010).

179. Bhate, S. S., Barlow, G. L., Schürch, C. M. & Nolan, G. P. Tissue schematics map the specialization of immune tissue motifs and their appropriation by tumors. *Cell Syst.* **13**, 109-130.e6 (2022).

Appendix II: Supplemental Figures

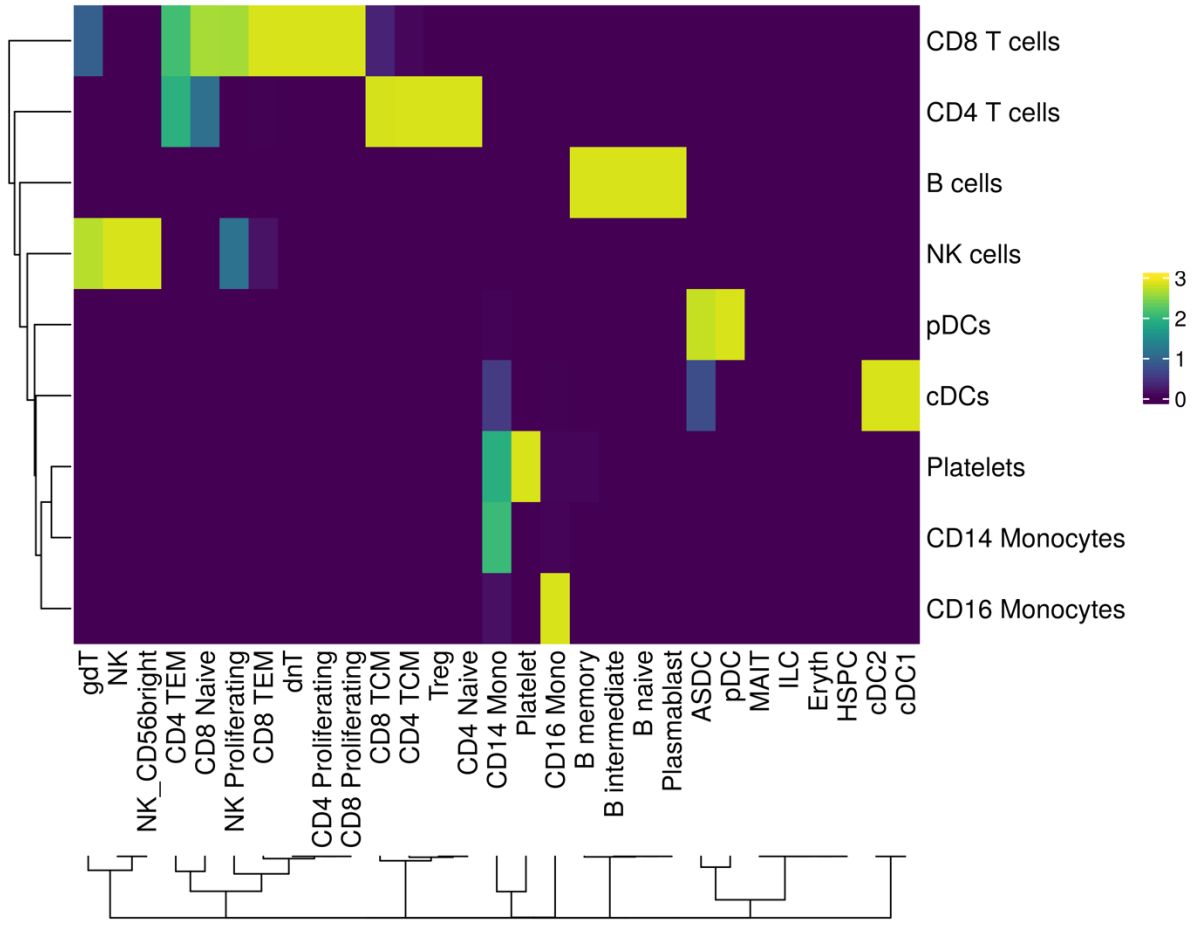

Supplemental Figure 1. Heatmap showing prediction scores between azimuth reference dataset and our clusters. Heatmap comparing our immune cell subsets identified using canonical markers to Seurat's Azimuth reference annotation. The heatmap color scale is based on Seurat's prediction score.

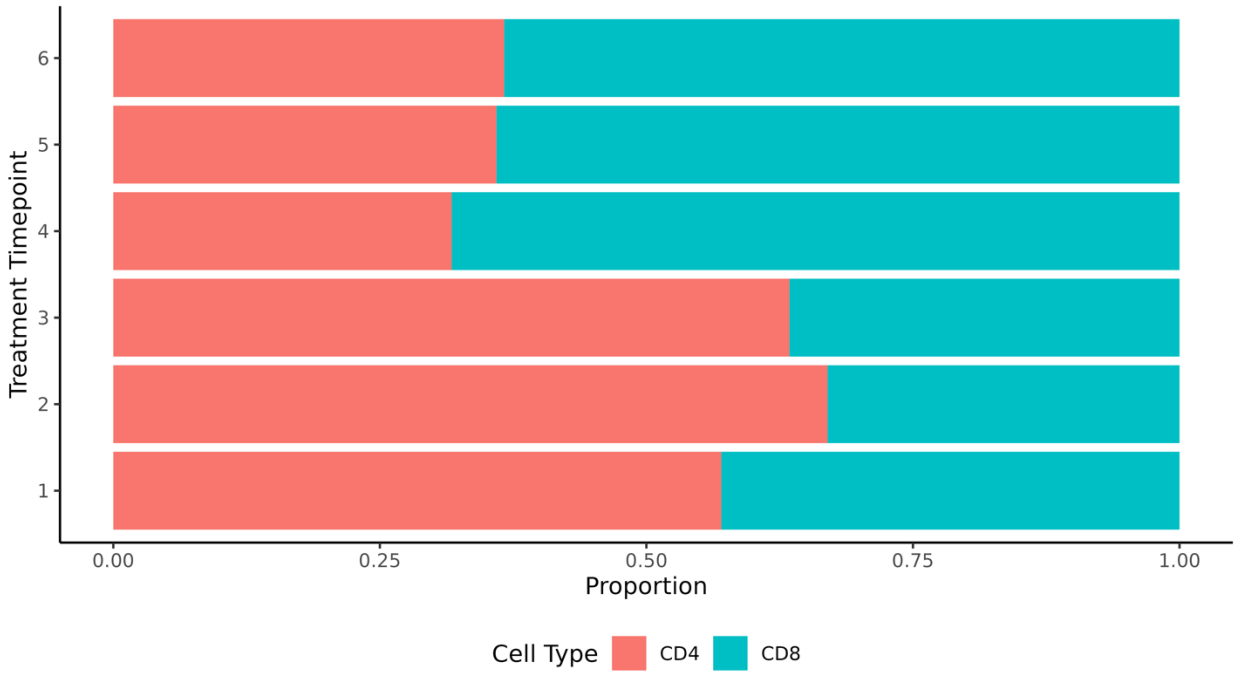

Supplemental Figure 2. CyTOF data showing proportion of CD4+ and CD8+ T cells across treatment timepoint. The proportion of CD4+ and CD8+ T cells subset from the entire PBMCs CyTOF dataset across each treatment time point.

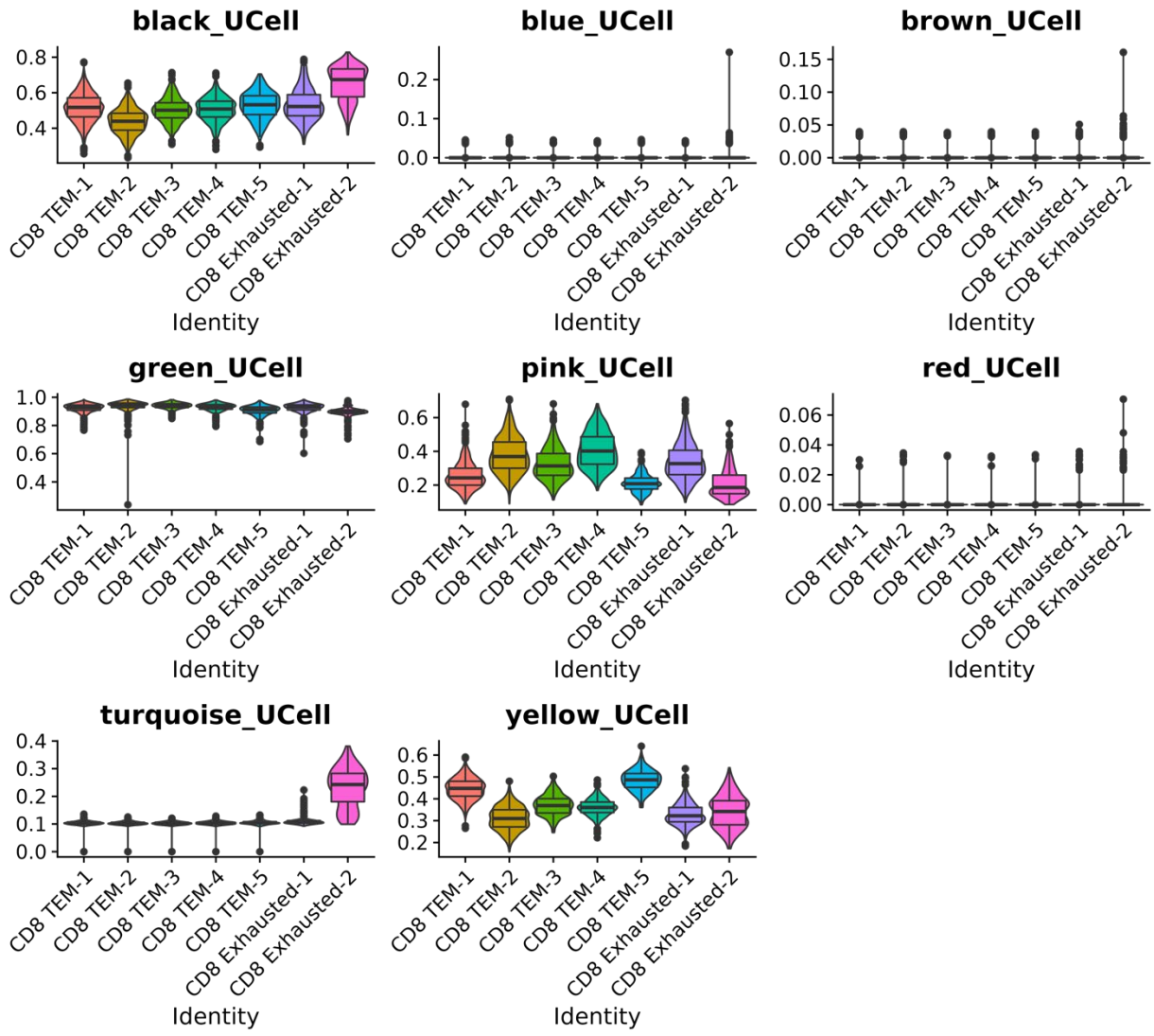

Supplemental Figure 3. Boxplot of WCGNA module scores across each CD8+ T cell cluster. Each module uncovered from WCGNA is represented by a color. We used UCell to calculate module scores for each CD8+ T cell cluster. UCell scores of each module are plotted as boxplots across each CD8+ T cell cluster.